Fractionation of Th-230, Pa-231, and Be-10 induced by particle size and composition within an opal-rich sediment of the Atlantic Southern Ocean

Fractionation of ^{230}Th, ^{231}Pa, and ^{10}Be induced by particle size and composition within an opal-rich sediment of the Atlantic Southern Ocean

Sven Kretschmer[1, 2*], Walter Geibert[3, 4], Michiel M. Rutgers van der Loeff [1],

Christoph Schnabel[5], Sheng Xu[5], Gesine Mollenhauer[1, 2]

[1] Alfred-Wegener-Institut für Polar- und Meeresforschung, Am Handelshafen 12, 27570 Bremerhaven, Germany

[2] Fachbereich Geowissenschaften, Universität Bremen, Klagenfurter Str., 28359 Bremen, Germany

[3] School of GeoSciences, University of Edinburgh, Edinburgh EH9 3JW, UK

[4] Scottish Association for Marine Science, Dunstaffnage Marine Laboratory, Oban PA37 1QA, UK

[5] Scottish Universities Environmental Research Centre, East Kilbride G75 0QF, UK

*Corresponding author: sven.kretschmer@awi.de, fax +49 471 4831 1425

Abstract

This study centers on the question: How sensitive are $^{231}Pa/^{230}Th$ and $^{10}Be/^{230}Th$ to sediment composition and redistribution? The natural radionuclides ^{231}Pa, ^{230}Th and ^{10}Be recorded in deep sea sediments are tracers for water mass advection and particle fluxes. We investigate the influence of oceanic particle composition on the element adsorption in order to improve our understanding of sedimentary isotope records. We present new data on particle size specific ^{231}Pa and ^{10}Be concentrations. An additional separation step, based on settling velocities, led to the isolation of a very opal-rich phase. We find that opal-rich particles contain the highest ^{231}Pa and ^{10}Be concentrations, and higher $^{231}Pa/^{230}Th$ and $^{10}Be/^{230}Th$ isotope ratios than opal-poor particles. The fractionation relative to ^{230}Th induced by the adsorption to opal-rich particles is more pronounced for ^{231}Pa than for ^{10}Be. We conclude that bulk $^{231}Pa/^{230}Th$ in Southern Ocean sediments is most suitable as a proxy for past opal fluxes. The comparison between two neighboring cores with rapid and slow accumulation rates reveals that these isotope ratios are not influenced significantly by the intensity of sediment focusing at these two study sites. However, a simulation shows that particle sorting by selective removal of sediment (winnowing) could change the isotope ratios. Consequently, $^{231}Pa/^{230}Th$ should not be used as paleocirculation proxy in cases where a strong loss of opal-rich material due to bottom currents occurred.

1. INTRODUCTION

1.1 Natural radionuclides and their application as proxies

The natural radionuclides ^{231}Pa, ^{230}Th, and ^{10}Be are powerful tracers, used to identify and quantify the transport of particles and of water masses in the ocean. The common property of Th, Pa, and Be in seawater is their particle reactivity, which makes them suitable for tracing past particle fluxes. They adsorb onto particles, sink out of the water column (scavenging), and are buried in the sediment. Pa and Be have a lower reactivity and consequently longer residence time than Th. This differing solubility creates disequilibria, and finally leads to isotopic ratios that differ from their production ratio, depending on their residence times in water column.

The production ratios of U-series nuclides are well defined. ^{230}Th (half-life 75,380 years) is produced by its progenitor ^{234}U in seawater (~2910 dpm m^{-3} at 35 permil salinity, Robinson et al., 2004) at a constant rate of 0.0267 dpm m^{-3} a^{-1} (François et al., 2004). Due to its strong particle reactivity (Langmuir and Herman, 1980), ^{230}Th is adsorbed to colloids or suspended particles shortly after its production in seawater (Moore and Hunter, 1985; Moore and Millward, 1988; Niven and Moore, 1993). The scavenging process for thorium is very efficient so that the rain rate of particulate ^{230}Th to the sea floor is nearly independent from the intensity of particle fluxes, and thus the vertical ^{230}Th flux is spatially and temporally constant and equals its production in the overlying water column (within an uncertainty of ±30 %, Henderson et al., 1999; Scholten et al., 2001). Therefore, the residence time of ^{230}Th in the water column with respect to scavenging is very short (10-40 years, Anderson et al., 1983a, 1983b). Due to its nearly constant vertical flux, the ^{230}Th concentration in sediments is

inversely related to the intensity of the vertical particle flux (Krishnaswami, 1976; Bacon, 1984; Suman and Bacon, 1989).

The source of ^{231}Pa (half-life 32,760 years) in seawater is the radioactive decay of ^{235}U at a constant rate of 0.0025 dpm m^{-3} a^{-1}. The activity ratio of ^{231}Pa/^{230}Th at the time of production from ^{235}U and ^{234}U is 0.093. However, protactinium is less reactive and has a longer scavenging residence time than thorium (10^2 years, Anderson et al., 1983a; 1983b). Therefore, ^{231}Pa/^{230}Th ratios may differ from the production ratio in response to the effects that lead to their removal and transport. In contrast to ^{230}Th, the distribution of dissolved ^{231}Pa is largely influenced by lateral mixing and advection of water masses that leads to its further transport and deposition in regions with enhanced particle fluxes (boundary scavenging, Anderson et al., 1983a, 1983b). Due to its sensitivity to the hydrography, the ^{231}Pa/^{230}Th ratio in sediments has been interpreted as a record of deep water ventilation in the Atlantic (Yu et al., 1996; McManus et al., 2004; Gherardi et al., 2009; Guihou et al., 2010; Negre et al., 2010; Guihou et al., in press).

As the ^{231}Pa/^{230}Th ratio is positively correlated to the intensity of particle fluxes (Yang et al., 1986), it has also been applied as an export productivity proxy (Kumar et al., 1993; Pichat et al., 2004). However, in the Southern Ocean the scavenging of ^{231}Pa has been found to be mainly controlled by opal flux (Rutgers van der Loeff and Berger, 1993; Walter et al., 1997). Therefore, in most recent studies located in high latitudes, the application of ^{231}Pa/^{230}Th has been restricted to reconstructing past changes of opal fluxes (Bradtmiller et al., 2007, 2009; Anderson et al., 2009), rather than total mass fluxes. It is still a matter of debate if the sensitivity of ^{231}Pa/^{230}Th ratios to particle composition affects their application as paleocirculation tracers, particularly in the North Atlantic. However, modeling results point to a significant role of particle composition for ^{231}Pa/^{230}Th records (Siddall et al. 2005), and the general lack of larger sets of observational data in combination with useful particle characterizations is hampering the reliable application of the proxy (Burke et al., 2011).

^{10}Be has a different production mechanism, but certain similarities to ^{231}Pa. Given its much longer half-life of 1.5 Million years, it could in principle serve as a welcome extension of the ^{231}Pa/^{230}Th proxy into to the more distant past. ^{10}Be is produced by spallation reactions in the troposphere (Lal and Peters, 1967; Lal 2002) at a globally averaged production rate of 1.2×10^6 atoms cm^{-2} a^{-1} at present (Monaghan et al., 1986). Once introduced to the ocean, ^{10}Be does not re-exchange with the atmosphere (Morris et al., 2002) but it is removed from the water column by scavenging to particles and burial in sediments (Finkel et al., 1977; Kusakabe et al., 1982; Lao et al., 1992). Owing to its residence time of ~500-1000 years, dissolved ^{10}Be is advected laterally in the ocean by water masses and preferentially scavenged and deposited in regions of high particle flux, similar to ^{231}Pa (boundary scavenging, Anderson et al., 1990). Long term records of ^{10}Be in marine sediments serve as a proxy for past variations in cosmic ray intensity and for the past geomagnetic dipole strength (Frank et al., 1997; Frank, 2000; Christl et al., 2007, 2010). ^{10}Be is also an important tool for sediment chronology (Bourles et al., 1989; Frank et al., 2008) and for the investigation of water mass advection (Ku et al., 1990; Frank et al., 2002; Luo and Ku, 2003). ^{10}Be normalized to the flux of excess ^{230}Th (^{10}Be/^{230}Th$_{xs}$) has been used for the reconstruction of variations in the past ocean productivity (Anderson et al., 1998). The ^{10}Be flux to marine sediments also varies as a function of lithology (Henken-Mellies et al., 1990; Chase et al., 2003).

1.2 The effect of sediment redistribution on nuclide ratios

It has been questioned to what extent the sedimentary ^{231}Pa/^{230}Th and ^{10}Be/^{230}Th records are determined by ventilation versus particle composition. Indeed, recent publications (Keigwin and Boyle, 2008; Scholten et al., 2008; Gil et al., 2009; Lippold et al., 2009) claimed that the distribution of ^{231}Pa/^{230}Th ratios is controlled at least partly by the abundance of diatoms and not by ventilation. Various studies have shown that thorium preferentially

adsorb on lithogenics and carbonates, beryllium on lithogenics and opal, whereas protactinium strongly prefers opal (Lao et al., 1993; Chase et al., 2002; Guo et al., 2002; Chase et al., 2003; Geibert and Usbeck, 2004). The disparity in adsorption behavior and past changes in particle composition may be disadvantageous for particle flux studies (Frank et al., 2000; Gil et al., 2009; Lippold et al., 2009), as it is one additional controlling factor on the tracer flux to the sediment, which may overprint the effect of other controlling factors (such as total particle flux or water mass advection) and complicate the interpretation of the sedimentary tracer records (Burke et al., 2011).

The opal-rich sediments of the Southern Ocean act as a sink for ^{231}Pa and ^{10}Be as a result from hydrography, scavenging residence times, and chemical composition of oceanic particles. Opal-rich sediments appear to be particularly susceptible to resuspension, which makes redistribution by strong abyssal bottom currents particularly important in the opal-belt of the Antarctic Circumpolar Current (Geibert et al., 2005). ^{231}Pa/^{230}Th and ^{10}Be/^{230}Th ratios have been commonly assumed to be insensitive to sediment redistribution, an assumption which remains to be proven. Focusing and winnowing of sediments occur under the influence of variable abyssal current velocities. Therefore, laterally transported sediment particles may be subject to a particle sorting according to particle size and hydrodynamic behavior (McCave et al., 1995). If distinct particle types with high and low isotope concentrations are decoupled from one another during a dislocation process, this may potentially change the particulate ^{231}Pa/^{230}Th and ^{10}Be/^{230}Th ratios in sediments after redeposition, which we can test as part of this study.

1.3 Approaches by other authors

Generally, data on oceanic ^{231}Pa and ^{10}Be are still scarce and beyond that, contrasting results led to discussions about their interpretation (Luo and Ku, 1999; Chase et al., 2002;

Chase and Anderson, 2004; Luo and Ku, 2004a, b). Therefore, a further development of $^{231}Pa/^{230}Th$ and $^{10}Be/^{230}Th$ as quantitative proxies needs more investigation. Various studies have investigated the scavenging and fractionation of ^{231}Pa, ^{230}Th, and ^{10}Be with respect to particle phases. These different approaches include field observations of geographical variability (e.g. Walter et al., 1997), scavenging experiments under controlled laboratory conditions (e.g. Geibert and Usbeck, 2004), correlations between radionuclides and sediment phases in surface sediments (e.g. Lao et al., 1992) or sediment cores (e.g. Henken-Mellies et al., 1990), studies on the partitioning between dissolved and particulate form in the water column by collecting suspended or settling particles (e.g. Chase et al., 2002), modeling studies (e.g. Siddall et al., 2005; Dutay et al., 2009; Luo et al., 2010), and finally component specific radionuclide analysis by physical or chemical isolation of particle fractions from sediments (e.g. Bourles et al., 1989; Luo and Ku, 1999; Lal et al., 2006).

The methods for component specific radionuclide analysis on isolated sediment fractions are challenging. The caveat associated with the selective chemical leaching of sediment phases is the risk of biasing due to desorption/adsorption kinetics of reactive nuclides from one phase to another (cf. Robinson et al., 2008). Physical separation of sediment phases by sieving and/or settling bears the problem of incomplete isolation of sediment phases (cf. Luo and Ku, 1999). The method of wet sieving also could produce an artifact by an unfavorable leaching of adsorbed isotopes and their loss to the sieving fluid. As a consequence the component specific radionuclides analyzed on mechanically/chemically isolated components may not be representative of their natural composition.

1.4 How this study addresses the problems

This paper contributes new data on component specific radionuclides in order to assess their sensitivity to redistribution. For our study, we selected two sediment samples (deglacial, 16

ka) from two neighboring sediment cores ("twin cores") from the Southern Atlantic Ocean, previously described by Kretschmer et al. (2010). While the twin cores are similar in most respects, they differ in the extent of sediment redistribution. The sample selection is also advantageous for our study because these samples are mainly composed of only two phases (opal and lithogenic). Carbonate particles contribute a negligibly small amount (<1 weight-%). We decided to physically separate those two sediment phases by a gentle treatment (i.e. without ultrasonication) with natural seawater so that the artificial chemical and physical influence on radionuclide distribution was reduced to a minimum. Any unfavorable leaching loss of radioisotopes to the sieve/settle fluid was monitored by analyzing the radioisotopes within the fluid. Particle separation was achieved by sieving into four size intervals, followed by a separation through settling velocity into fast and slowly settling particle classes. The fast settling class mainly contains particles of lithogenic source (higher specific density) and the slowly settling class mainly contains particles of biogenic opal (lower specific density). Even though this physical separation was incomplete, the resulting sediment fractions carry radioisotope signatures that are strongly differing. Kretschmer et. al (2010) had studied ^{230}Th U and Th in the same size and density fractions of the two cores analyzed in this study, the new results in this manuscript are on ^{231}Pa and ^{10}Be. This paper describes and compares the distribution of radioisotopes within the sediment samples and the influence of biogenic opal on the ^{231}Pa/^{230}Th and ^{10}Be/^{230}Th ratios. The influence of focusing and winnowing on the isotope ratios and the implication on their use as kinematic proxy for deep water ventilation is discussed.

2. MATERIALS AND METHODS

2.1. Sediment core location

Two neighboring sediment cores located in the Southern Ocean opal belt, Atlantic sector south of the Antarctic Polar front (APF), equal in water depth, but different in sedimentation rates were selected for comparison. These two gravity cores (PS1768-8 and PS1769-1) were recovered during Polarstern cruise ANT-VIII/3 at 52.5930°S, 4.4760°E, 3299 m water depth and at 52.6125°S, 4.4580°E, 3269 m water depth, respectively. The sediment composition is dominated by diatomaceous mud and ice rafted debris (Gersonde and Hempel, 1990). Despite the only 2.5 km lateral distance between the twin cores, they reveal contrasting accumulation rates. The sediment deposition during the last deglacial at core site PS1768-8 (mass accumulation rate (MAR)=10.1 g cm^{-2} ka^{-1}, focusing factor (Ψ)=5.9; Frank et al., 1996) is twice as high as at core site PS1769-1 (MAR=4.4 g cm^{-2} ka^{-1}, Ψ=3.2; Kretschmer et al., 2010), which is assumed to result from lateral sediment transport by bottom currents. The age model of core PS1768-8 is constrained by a combination of oxygen isotope stratigraphy, siliceous microfossil biofluctuation stratigraphy and radiocarbon dating (Frank et al., 1996). Age control for core PS1769-1 was obtained by correlating the magnetic susceptibility record to that of the parallel core. Each of the twin cores was sampled at one core depth (PS1768-8 at core depth 166-169 cm; PS1769-1 at core depth 14-16 cm) representing the last deglacial period (16 ka).

2.2. Grain size fractionation

The procedure of the grain size fractionation is reported in detail by Kretschmer et al. (2010). The fractionation of two sediment samples into grain size classes was achieved by wet

sieving and settling. Natural seawater (sea surface from the North Sea) was used as sieving fluid in order to prevent artifacts such as dissolution of particles or desorption of radionuclides that could result from using deionized water. In order to avoid artifacts from particles contained in the natural seawater, it was filtered through polycarbonate-filters (pore size 1 µm) before using it as a sieving fluid. As this natural seawater contains also radionuclides of Th, Pa, and Be, which may produce artifacts to the results, the concentration of radionuclides in the sieving fluid was monitored before and after sediment sieving, as described in section 2.2.2.

The two sediment samples were suspended in filtered seawater and agitated for 2 minutes. The samples were separated into particle size-classes by wet sieving using three nylon sieves (mesh 125 µm, 63 µm, 20 µm). Each of the resulting particle size-classes consisted of particles with different specific densities, i.e. biogenic silica particles (low density) and lithogenic particles (high density). The size and specific density of a particle determine its settling velocity and hence its hydrodynamic behavior in a natural marine system. Therefore, the low density biogenic opal particles were separated from the high density lithogenic particles by their settling velocity in seawater, so that the three sieve fractions 20-63 µm, 63-125 µm, and >125 µm were each split into a "slowly settling" and a "fast settling" fraction. Two settling velocities were specified: the maximum terminal velocity (fast sinking particles) was estimated assuming the average density of quartz (2.65g cm^{-3}), the minimum terminal velocity (slowly sinking particles) was determined empirically by measuring settling times of the slowest particles in a settling tube with seawater. Shortly after the fast particles settled down to the bottom of the settling tube the slowly particles were siphoned off. The fraction that rapidly settled to the bottom was again suspended and the separation process was repeated (15-20 times) until the supernatant fluid appeared clear.

The separation of the <20 µm-fraction into clay-sized particles (<2 µm) and silt-sized particles (2-20 µm) was impossible when using seawater, as the smallest particles were

flocculating due to the presence of cations in seawater. For further fractionation into the classes <2 µm and 2-20 µm based on the settling velocity principle the <20 µm-fraction was resuspended in purified water. After a certain settling time (calculated by Stokes' law), the clay-sized fraction (<2 µm) remaining in suspension was siphoned off, while the fine silt fraction (2-20 µm) settled out from suspension to the bottom of the settling tube and was again resuspended in purified water. This procedure was repeated 10-20 times until the supernatant fluid achieved a low turbidity. Due to the repeated decantations the clay-sized fraction (<2 µm) was recovered in a large volume of water. As flocculation reagent, a $CaCl_2$-solution was added for extracting all particles from the water. The flocculated particles were allowed to settle down for four days, and then supernatant was decanted and stored separately in a canister for further processing (section 2.2.2).

2.2.1 Characterization of the grain size fractions

Further analyses of the sediment fractions include the measurement of biogenic opal (bSi), specific surface area (SSA), and element concentrations. Results were reported by Kretschmer et al. (2010) and are listed in the appendix in Tables A2 and A3.

The determination of biogenic opal (bSi) followed the description of Müller and Schneider (1993) where opal was extracted with NaOH (1 M) at 85°C, and dissolved silica was continuously analyzed by molybdate-blue spectrophotometry. The main characteristic of the slowly settling particles is its high concentration of biogenic opal (mainly diatom tests, 75-82 wt-%). Also the fine silt (2-20 µm) and the clay-sized (<2 µm) particle fractions contain high amounts of opal (mainly fragments of diatom tests, 76-80 wt-% respectively 61-68 wt-%). In contrast, the fast settling particles with lower opal content (3-17 wt-%) contain mainly ice rafted rock fragments, mixed with radiolarians and few diatoms.

Element concentrations (Be, Al, Fe, Mn) have been analyzed on the samples after full acid digestion using the ICP-SF-MS Element2 (Thermo Scientific). Calibrations were done with certified standard solutions and external reproducibility was monitored using the NIST standard reference material 2702 (inorganics in marine sediment). Fe-Mn oxyhydroxides in the form of coatings or micronodules are known to scavenge both Pa and Th (Anderson et al., 1983a and references therein; Anderson et al., 1994; Roy-Barman et al., 2005, 2009) and could therefore play an important role for the grain size distribution of isotopes in sediments. However, we have no evidence for the existence of Fe-Mn oxyhydroxides in the samples analyzed. It seems that Fe-Mn oxyhydroxides are of minor importance for our study as concentrations of Fe and Mn show no correlation to concentrations of Th, Be or Pa. Data on Fe and Mn were reported by Kretschmer et al. (2010).

The specific surface area [$m^2\ g^{-1}$] of sediment fractions from PS1769-1 was determined by gas adsorption analysis on a Quantachrome *Nova 2200*. The sediment samples were degassed and heated (110°C for 2h) to remove surface adsorbed water. After evacuation, the sediment was subjected to five partial pressures of N_2 gas (purity 99.996%) and the surface area was calculated using the BET-theory (Brunauer et al., 1938) according to ISO9277.

2.2.2 Seawater processing

The use of natural seawater as sieving fluid could provoke artifacts on the radionuclide concentrations on the sieved sediment particles resulting from adsorption- or desorption-effects. Therefore radionuclide concentrations were determined in the sieving fluid before it was used for the wet sieving process (i.e. “unused” seawater) and after the wet sieving of the sediment samples. The seawater used for wet sieving was collected in canisters (between 11 L and 22 L per sieved sample, Table 1). Prior to analysis, all seawater samples were acidified

(pH 2-3) by addition of nitric acid (HNO_3). The yield tracers ^{229}Th, ^{233}Pa, ^{236}U, ^{9}Be, and a solution of iron chloride were added. After time for equilibration (24 h) ammonium hydroxide (NH_4-OH) was added to adjust a pH 8-9 for co-precipitating the radionuclides with iron hydroxide ($Fe(OH)_3$). The precipitate was re-dissolved in HNO_3 and ion exchange chemistry was performed following the same protocol as for the sediment samples (section 2.3).

The results in Table 1 show that after sediment sieving the radionuclide concentrations in the sieving fluid were higher than before sieving. The difference is assumed to be the amount that was leached from sediment during the sieve/settle process. It accounts for 0.4-2.4 % relative to the total amount of ^{230}Th, ^{231}Pa and ^{10}Be within the respective bulk sample.

2.2.3 Recovery of ^{230}Th, ^{231}Pa, and ^{10}Be during sediment sieving

The isotope recoveries after sediment sieving are calculated by summing up the ^{230}Th, ^{231}Pa, and ^{10}Be concentrations of all particle size fractions and dividing by the concentration of the respective bulk sample. Recoveries of ^{230}Th, ^{231}Pa, and ^{10}Be in sediment fractions sum up to, respectively, 87-90 %, 109-110 %, and 103-104 % relative to the bulk sample (Table 1).

[We suggest setting the following section 2.3 in small print]

2.3. Radioisotope analyses

The analyses of ^{231}Pa, ^{230}Th, and ^{10}Be were performed in the laboratories of the Marine Geochemistry department at Alfred-Wegener-Institute, Bremerhaven, Germany and the NERC Cosmogenic Isotope Analysis Facility (CIAF) and AMS laboratory, both at the Scottish Universities Environmental Research Center (SUERC), East Kilbride, UK. These laboratories participated in the GEOTRACES inter-calibration program for ^{231}Pa, ^{230}Th and

^{10}Be (Henderson et al., 2007). The data on ^{231}Pa ($T_{1/2}$=32.5 ka), ^{230}Th ($T_{1/2}$=75.4 ka), and ^{10}Be ($T_{1/2}$=1.5 Ma) reported in this manuscript are decay-corrected for the time of deposition. All data are available at doi:10.1594/PANGAEA.759976.

2.3.1. ^{231}Pa sample preparation and ICP-MS

For the isotope dilution analysis by Inductively Coupled Plasma-Sector Field-Mass Spectrometry (ICP-SF-MS) the samples were spiked with ^{229}Th, ^{233}Pa and ^{236}U. The protactinium spike ^{233}Pa was produced from a ^{237}Np solution by separating ^{233}Pa from its progenitor by chromatography on a silica gel column. The spikes ^{229}Th, ^{233}Pa and ^{236}U were calibrated against the reference standard material UREM 11, an uranium ore. Hansen and Ring (1983) established that this material is in state of radioactive equilibrium. The consensus value for the uranium concentration in UREM 11 is 58.9±0.5 ppm (Hansen and Ring, 1983). From this value, we deduced the concentrations of ^{238}U (58.48±0.50 ppm), ^{234}U (3.16±0.03 ng g^{-1}) and ^{235}U (418.8±3.6 ng g^{-1}) and calculated the concentrations of the respective daughter nuclides ^{230}Th (957.3±8.2 pg g^{-1}) and ^{231}Pa (19.16±0.16 pg g^{-1}).

Samples (10-100 mg) and spikes (0.7 pg ^{233}Pa, 9 pg ^{229}Th, and 800 pg ^{236}U) were weighed into Teflon vials and fully dissolved in HCl, HNO_3, and HF by microwave-assisted digestion (CEM Mars Xpress). Samples were evaporated to dryness, re-dissolved, and co-precipitated with $Fe(OH)_3$. Separation of Pa, Th and U was achieved by ion exchange chromatography with two different exchange resins (Eichrom UTEVA® and BioRad AG 1-X8®). The UTEVA columns were conditioned with three column volumes (cv) HNO_3 (3M), then loaded with the samples and rinsed with HNO_3 (3cv 3M). Th was eluted with HCl (1cv 9M and 2cv 5M suprapur®) followed by elution of Pa and U with 3cv HCl (0.02M) + HF (0.02M suprapur®). The eluates were collected and evaporated in Teflon beakers. The Th fraction was re-dissolved in HNO_3 and as the last step diluted to 5 mL HNO_3 (1M). The Pa-U

fraction was re-dissolved in HCl (9M). The AG 1-X8 columns were conditioned with HCl (9M) and loaded with the Pa-U fraction. The first rinsing (3cv HCl 9M) cleaned the column from any remaining Th and was discarded. Subsequently it was collected for Pa (3cv HCl 9M + HF 0.14M) and for U (5cv HCl 0.5M). The separated Pa and U fractions were evaporated and re-dissolved in HNO_3 twice, and finally diluted to 5 mL HNO_3 (1M).

Isotopes of Pa, Th and U were analyzed by isotope dilution using ICP-SF-MS (Element2, Thermo Scientific). Samples were injected into the plasma by a desolvation system (Apex Q®, ESI). During the injection of the Pa fraction, Th hydride ($^{232}ThH^+$) formation may contribute to the mass 233. This was reduced to a minimum by optimizing the sample and Argon gas flow rates and the plasma temperature. In addition, the ^{232}Th peak tailing contributes to the masses 233 and 231. The external measurement of a ^{232}Th standard solution allowed the assessment of these analytical effects. The contribution to masses 231 and 233 by $^{232}ThH^+$ and ^{232}Th peak tailing was corrected by measuring the ^{232}Th in each Pa sample. The instrument mass bias was assessed externally by bracketing samples with a uranium standard solution. Further corrections accounted for ^{233}U bleeding (traced by ^{236}U) and procedural blanks. Procedural blanks (including spike contribution) were equivalent to 0.8-3% (^{231}Pa) and 0.6% (^{230}Th) of the samples.

The scavenging process is the principal source for ^{230}Th and ^{231}Pa in sediments. Additionally, two further sources contribute variable small amounts to the total ^{230}Th and ^{231}Pa in sediments: ^{230}Th and ^{231}Pa that is supported by decaying uranium in lithogenic minerals, and by decaying uranium from authigenic source. For particle flux studies, only the scavenged component of ^{230}Th and ^{231}Pa is of interest, i.e. the total ^{230}Th and ^{231}Pa measured in sediments must be corrected for the other two components. The scavenged fraction is referred to as "excess" (excess ^{230}Th or $^{230}Th_{xs}$ and excess ^{231}Pa or $^{231}Pa_{xs}$) and must be decay corrected for the time of deposition which requires an independent chronology for the sediment core (Henderson and Anderson, 2003).

2.3.2. *^{10}Be sample preparation and AMS*

^{10}Be was analyzed on 12 sediment samples (2×bulk + 10×fractions) and four seawater samples. The size classes <2 µm and 2-20 µm were not analyzed separately but were combined for a measurement of the fraction <20 µm. The size classes 63-125 µm and >125 µm were combined for a measurement of >63 µm. About 390 µg Be (in 3 wt-% HNO_3) was added to the sediment samples (~100 mg) prior to the microwave-assisted full acid digestion. After sample digestion, the acid was fumed off until dryness and samples were re-dissolved in HCl (3 mL, 6 M) twice. The four acidified (pH 2-3) seawater samples (2×supernatant sieving fluid and 2×"unused" seawater, for details see section 2.2.2) were prepared for ^{10}Be measurement by adding 2 mL solution of iron chloride ($FeCl_3$ in HCl, 50mg/mL) and 390 µg Be (in 3 wt-% HNO_3). After 24 h of equilibration aqueous ammonia was added until pH 10 was reached and Be was co-precipitated with $Fe(OH)_3$ and $Mg(OH)_2$. The supernatant was siphoned off and the precipitate was re-dissolved in HCl. After three times of co-precipitations the sample volume was ~30 mL. It was further reduced to ~3 mL by evaporation on hotplates.

Samples (in HCl, 3 mL, 6 M) were loaded on basic anion exchange resin (Merck, Dowex 1-X8, 2 mL), eluted with HCl (3 cv, 6 M), and immediately collected for Be. Fe is bound to the resin as $FeCl_4^-$-anion. As the Fe content in the seawater samples was very high due to the $Fe(OH)_3$-co-precipitation, each seawater sample was split into two fractions and anion exchange was repeated using a large column (5 mL resin) for each sample split. After anion exchange the sample splits were combined again before the next step.

Samples were converted into sulfate form by adding H_2SO_4 (1 mL 0.5 M, analytical grade) and evaporating to near dryness. H_2O_2 (6 drops 2 wt %) and H_2SO_4 (2 mL 0.04 M) were added and evaporated two times to a syrupy droplet. The sample was re-

dissolved in H_2SO_4 (2 mL 0.04 M), let stand overnight and centrifuged before loading to the cation exchange columns. The "fast settling" particle fractions were estimated to contain high cation loads (particularly Na^+, Mg^{2+}, Ca^{2+}, Al^{3+}, and TiO^{2+}), so that they were split onto two columns (each 2 mL) in parallel. All other samples were separated on one column. Samples were loaded on a sulfonic acid cation exchange resin (BioRad, AG 50W-X8 Resin, 2 mL, 200-400 mesh) conditioned with 0.2 M H_2SO_4. Then the TiO^{2+}-containing fraction was eluted from the resin with H_2SO_4 (6 cv 0.5 M), followed by elution of Be^{2+} with HCl (5 cv 1.2 M), and Al^{3+} was removed from the resin with HCl (3 cv 4.5 M).

The Be-fraction was reduced to a small volume (~1 mL) by evaporation and $Be(OH)_2$ was precipitated at pH 9 by adding an aqueous NH_3 solution (25 wt-%). The precipitate was centrifuged and washed with pH 7 solution (1 mL) three times, dissolved in concentrated HNO_3 (60 µL 70 %, certified) and transferred to quartz crucibles. Samples were dried down on a hotplate, and $Be(NO_3)_2$ was partly decomposed by increasing the temperature to above 200°C. For conversion to BeO the samples were heated in a furnace to 900°C.

For the AMS analysis BeO was mixed with Niobium (~4 mg, purity 99.99%, Alfa Aesar, 325 mesh; mixing ratio BeO/Nb = 1:6 wt/wt) and pressed into a Cu cathode. The $^{10}Be/^{9}Be$ ratios that resulted after carrier addition were measured with the 5 MV accelerator mass spectrometer at SUERC (Freeman et al., 2007). The measurement is described in detail by Xu et al. (2010). NIST SRM4325 with a $^{10}Be/^{9}Be$ ratio of 3.06×10^{-11} (Middleton et al., 1993) was used for normalization.

3. RESULTS AND DISCUSSIONS

3.1. Protactinium

The fast sinking coarse particles >20 µm (opal-poor) are characterized by very low $^{231}Pa_{xs}$ specific activities (0.03±0.01 - 0.19±0.03 dpm/g, Figure 1, Table A1 in the Appendix), and by $^{231}Pa_{xs}/^{230}Th_{xs}$ activity ratios (0.013±0.003 - 0.05±0.01) lower than the production ratio (0.093). In contrast, the slowly sinking coarse particles >20 µm (opal-rich) and the fine particles <20 µm (opal-rich) reveal high specific activities (0.46±0.08 - 1.89±0.32 dpm/g) and their $^{231}Pa_{xs}/^{230}Th_{xs}$ activity ratios (0.11±0.03 - 0.54±0.13) are similar to or higher than the production ratio.

Bulk $^{231}Pa_{xs}$ activities (1.10 ± 0.19 dpm/g, Figure 1) are in agreement with $^{231}Pa_{xs}$ data from Frank et al. (2000) who report for the same sediment core PS1768-8 at similar core depth (156-181 cm) a decay corrected $^{231}Pa_{xs}$ activity of 1.37 ± 0.27 dpm/g analyzed with alpha spectrometry. Bulk $^{231}Pa_{xs}/^{230}Th_{xs}$ ratios (0.16±0.04) are within the range of previously published ratios (0.12-0.24) reported for the glacial Southern Ocean on sediment cores just south of the Antarctic polar front (APF) close to our core site by Kumar et al. (1995) and Anderson et al. (1998).

3.2. Beryllium

3.2.1 $^{10}Be/^{230}Th$ distribution by particle type

The fast sinking coarse particles >20 µm (opal-poor) are characterized by ^{10}Be concentrations (0.50±0.02 - 0.86±0.03 × 10^9 at/g, Figure 1, Table A2 in the Appendix) and $^{10}Be/^{230}Th_{xs}$ ratios (0.21±0.04 - 0.33±0.06 × 10^9 at/dpm) lower than within all other particle

classes. The slowly sinking coarse particles >20 µm (opal-rich) reveal ^{10}Be concentrations (0.84±0.03 - 1.33±0.04 × 10^9 at/g) slightly higher than the fast sinking particles, but their ^{10}Be/^{230}Th$_{xs}$ ratios (0.49±0.08 - 0.57±0.10 × 10^9 at/dpm) are the highest of all. In contrast, the fine particles <20 µm (opal-rich) carry the highest ^{10}Be concentrations (3.03±0.09 - 3.11±0.10 × 10^9 at/g), but their ^{10}Be/^{230}Th$_{xs}$ ratios (0.39±0.07 - 045±0.08 × 10^9 at/dpm) are equal (within errors) to the slowly sinking classes. ^{10}Be/^{230}Th$_{xs}$ ratios in all particle size classes exceed the production ratio in seawater (0.136-0.170 × 10^9 at/dpm).

Within the same core PS1768-8 at similar core depth (156-181 cm) Frank et al. (2000) analyzed the ^{10}Be concentration by chemical leaching of the sediment and report a ^{10}Be concentration of 1.23±0.04 × 10^9 at/g. This is half the concentration of what we measured by complete acid digestion (2.5±0.1 × 10^9 at/g, Figure 1). Either a higher ^{10}Be signal by complete digestion may derive from a lithogenic ^{10}Be source or the recovery of authigenic ^{10}Be from marine sediments by acid leaching may be incomplete (Bourles et al., 1989). The cause for the discrepancy of both ^{10}Be data cannot be clarified here. In the following paragraph however, the ^{10}Be sources are discriminated by using the ^{10}Be/Be ratio within the particle fractions.

3.2.2 Origin of the ^{10}Be/Be signal

It has been shown that dissolved trace metals are trapped within the silica structure of diatoms so that past metal concentrations in surface waters are recorded by sedimentary opal tests (Lal et al., 2006). This idea is supported by the observation of ^{10}Be depletion in surface waters of the modern Atlantic ACC which is suggested to result from enhanced scavenging by opal particles in the euphotic zone (Frank et al., 2002). Following this line of argument, our slowly settling opal-rich 20-63 µm particle fractions of PS1768 and PS1769 (containing 75 and 82 % biogenic opal, Table A3) largely reflect an authigenic surface water derived ^{10}Be/Be

signal (respectively 4.26±0.14 and 4.10±0.17 × 10^{-8} at/at, Figure 1). Assuming that ^{10}Be/Be is equal within all opal tests in all size fractions of PS1768 and PS1769 we can calculate the ^{10}Be/Be ratios for pure (i.e. 100 %) biogenic opal to be 5.7±0.2 and 5.0±0.2 ×10^{-8} at/at respectively. The fine particle fractions (<20 µm, clay and fine silt) of PS1768 and PS1769 reveal slightly higher ^{10}Be/Be ratios (5.46±0.19 and 5.54±0.20 × 10^{-8} at/at, respectively) than slowly settling opal-rich >20 µm particles, but they contain less biogenic opal (55 % and 58 %, respectively). We, therefore, suspect that a significant portion of ^{10}Be/Be must have been contributed by the lithogenic component of the fine fraction (i.e. clay and fine silt). Based on the ^{10}Be/Be ratios calculated for the pure biogenic opal we can calculate the ^{10}Be/Be ratios in the pure lithogenic fine fraction to be 5.2±0.3 and 6.3±0.3 ×10^{-8} at/at. The deep and bottom water could be a possible source for ^{10}Be adsorbed onto clay and fine silt. The ratio reported for the modern deep and bottom water of the circumpolar current is about 10-11×10^{-8} at/at (Kusakabe et al., 1987). Regarding the modern oceanography, it has been suggested that only an advection of ^{10}Be from the deep Pacific could explain the high ^{10}Be concentrations in the deep water of the Atlantic sector of the Southern Ocean (Frank et al., 2002). Furthermore, the sedimentary clay mineral assemblage of the Eastern South Atlantic sediments indicates a long distance transport of lithogenic material originating from Patagonia and the Antarctic Peninsula (Diekmann et al., 1996). Thus we interpret the high ^{10}Be concentrations found in the <20 µm-fraction to be partly derived from the adsorption on clay minerals that are advected by bottom currents from distant sources. However, if ^{10}Be/Be was, as it is today, even higher in the deep and bottom water than measured in our lithogenic fraction then the lithogenic component may be diluted with a lower^{10}Be/Be ratio deriving from aeolian dust that may range from 0.1 to 2×10^{-8}, as reported for surface soils (Barg et al., 1997). The absolute ^{10}Be contribution to the deep water by aeolian dust is insignificant (Wang et al., 1996), acting mainly as a diluting agent. Dust fluxes of 1-5 g/m^2/y have been reported from ODP core 1090 (Martínez-Garcia et al., 2009).

Lal et al. (2006) analyzed $^{10}Be/Be$ in cleaned opal samples that were separated from sediments (5.8 ka - 125 ka) from the ODP core 1093 located very close to our core site. The $^{10}Be/Be$ ratios in these opal tests widely range between 0.19 and 50×10^{-8} at/at and the error associated with the $^{10}Be/Be$ data can be as high as 20 %. If such large uncertainties are taken into account for our study, the differences of $^{10}Be/Be$ between particle fractions as discussed above would be insignificant. Nevertheless, the data of the <20 µm fraction demonstrate that lithogenic fines substantially contribute to the $^{10}Be/Be$ signal so that our conclusion is still valid, i.e. that ^{10}Be at our study site partly derived from sources other than the ocean surface water.

3.3. Influence on isotope ratios by sediment redistribution

Comparing the rapid with the slow accumulation site (Figure 1, white and black bars, respectively) they mostly reveal identical (within 1σ) isotope concentrations and ratios. Systematic differences between both sites are not observable. Both sites probably receive particles of the same composition that experience the same water masses, owing to their close neighborhood and the similar water depth. We conclude that mass accumulation rates and consequently the total fluxes of Pa, Th and Be may differ widely between two study sites under contrasting focusing conditions on local scale without affecting their respective isotope concentrations and ratios.

To assess the potential size sorting effect on the isotope signal of the sediments Table 2 provides the percentage of isotopes contributed by each size class in relation to the total inventories. The fine grained (<20 µm) and slowly settling opal-rich particles are the main contributors to the isotope inventories and therefore they determine the sedimentary isotope ratios. The size fraction (<20 µm) contributes 88-91 % of the total amount of the radioisotopes in the sediment samples. The differences in contribution by the <20 µm-fraction

are rather small for the three radioisotopes. The opal-rich particle class of size 20-63 µm is also an important carrier for the three radioisotopes. This class holds more $^{231}Pa_{xs}$ (9-10 %) than ^{10}Be (5-7 %) and $^{230}Th_{xs}$ (4-6 %). These differences are essential for the change in isotope ratios in the case of particle sorting by bottom currents as shown in the following paragraph.

Figure 4 illustrates a simulation of winnowing by progressively removing the fine sediment component and calculating the resulting radioisotope composition. Two scenarios for winnowing are shown in Figure 4. The removal of only the finest fraction (<20 µm, dashed line) leads to a slight increase of the $^{231}Pa/^{230}Th$ and the $^{10}Be/^{230}Th$ ratios compared to the measured bulk composition. The removal of the finest fraction (<20 µm) together with the slowly settling opal-rich particles (solid line) leads to decreasing isotope ratios. Among those two simulations we expect the second one being the more realistic scenario because the finest particles and the opal particles are both quite susceptible to resuspension and transport owing to their hydrodynamic behavior. A substantial removal of the fine and opal-rich particles (reduction of 70 to 80 % relative to the bulk composition) would reduce the $^{231}Pa/^{230}Th$ ratio to a value lower than the production ratio (0.093). $^{10}Be/^{230}Th$ ratios would also be affected by winnowing, but less pronounced than $^{231}Pa/^{230}Th$. Consequently, strong winnowing at our study site could fractionate ^{230}Th, ^{231}Pa, and ^{10}Be.

The opposite will happen in case of concentration of the fine and opal-rich particles by a stronger focusing. However, this stronger focusing could not change significantly the isotope ratios because the investigated cores are already strongly determined by the redistributed fines (<20 µm) and slowly sinking opal-rich particles making 87-91% of the sediment (Table 2) so that the sediment setting is much closer to the full-focusing extreme than to the situation of winnowing. That means that a stronger focusing would hardly change the isotope ratios.

However, regarding the sedimentary setting (strong sediment focusing during glacial and interglacial; Frank et al., 1996), events of strong winnowing are rather unusual at our study site. Therefore, an influence of particle sorting on isotope ratios would more probably occur in regions of strong winnowing, such as, e.g., reported for places south of the Subantarctic Front between 46°S and 48°S (Frank et al., 1996).

We can conclude that moderate variations in fluxes of particulate Th, Be, and Pa by lateral advection have negligible influence on the sedimentary isotope ratios found at our study site, and that the isotope ratios reflect particle fluxes on local scale independent of the mass accumulation rate. This conclusion is only valid if redistribution occurs syndepositionally and over short distances. In the case of long range particle transport as already indicated by the ^{10}Be data any reliable location-specific information on past fluxes of certain particle types cannot be provided.

3.4. Influence of opal content on isotope ratios

$^{231}Pa_{xs}$, ^{10}Be, and $^{230}Th_{xs}$ concentrations are positively correlated to the specific surface area, reflecting the adsorptive binding of all three nuclides to the surfaces of particles (Figure 2a). The ratios $^{231}Pa_{xs}/^{230}Th_{xs}$ and $^{10}Be/^{230}Th_{xs}$ are positively correlated with the biogenic opal content of the particles (Figure 2b) confirming findings of earlier studies (Taguchi et al., 1989; François et al., 1993; Asmus et al., 1999; Chase et al., 2002; Bradtmiller et al., 2009). In contrast, the isotope ratios show an anti-correlation to Al (Figure 2b). This is expected as Al represents the lithogenic component which is anti-correlated to biogenic opal. We conclude that the capacity of element adsorption is a function of the surface area of the particle, whereas the ability to fractionate between elements depends on the opal content of the particle.

The consequence is, that in regions where biogenic opal is dominating the particle flux $^{231}Pa_{xs}/^{230}Th_{xs}$ cannot reliably indicate neither the ocean ventilation nor the total mass flux. Thus its use as kinematic proxy and paleoproductivity proxy is limited in those situations. This confirms the statements of earlier studies (e.g. Walter et al., 1997; Keigwin and Boyle, 2008; Scholten et al., 2008; Lippold et al., 2009). Such effects of particle composition on sediment $^{231}Pa/^{230}Th$ can be taken into account by analyzing the opal content of the sediment (Gherardi et al., 2009; Guihou et al., in press). Luo et al (2010), however, demonstrate by a 2-D model approach, that a change of particle composition in the Southern Ocean could change the Southern Ocean ^{231}Pa sink and consequently the sediment $^{231}Pa/^{230}Th$ in the Atlantic basin.

In order to test whether the fractionation by opal content is stronger for either one of the nuclides ^{231}Pa or ^{10}Be, we introduce the distribution ratio $D(N/Th)$ as a new parameter. As $D(N/Th)$ is a ratio of percentages, the direct comparison between the Pa-Th- and Be-Th-fractionation is possible and independent of units. The percentage (i.e. the fraction:bulk ratio) of the nuclide N (^{231}Pa or ^{10}Be) within a certain particle size class is divided by the percentage of ^{230}Th within the same particle size class (equation 1),

$$D(N/Th) = [N_{fraction}/N_{bulk}] / [Th_{fraction}/Th_{bulk}], \quad (1)$$

where N is the concentration of either $^{231}Pa_{xs}$ or ^{10}Be, and Th is the concentration of $^{230}Th_{xs}$. Deviation of $D(N/Th)$ from 1.0 reflects adsorption intensities of N different from that of Th. $D(N/Th)>1$ indicates preferential adsorption and $0<D(N/Th)<1$ indicates less adsorption of N relative to Th. The $D(N/Th)$ ratio is displayed in Figure 3 on a logarithmic scale where bars are sorted from left to right by increasing opal content. As expected, preferential scavenging of Th relative to Pa and Be is found in the opal-poor particles ($D(N/Th)$=0.2-0.9), whereas the inverse situation is found within the opal-rich particle classes ($D(N/Th)$=1.3-3.3). Within all

particle classes, $D(^{10}Be/^{230}Th)$ is closer to unity than $D(^{231}Pa/^{230}Th)$. That means the fractionation between ^{230}Th and ^{10}Be is less sensitive to the opal content than the fractionation between ^{230}Th and ^{231}Pa. This is consistent with results of other investigators suggesting that ^{10}Be scavenging is sensitive to both opal and lithogenic particles fluxes (e.g. Lao et al., 1992; Frank et al., 2000; Chase et al., 2002), whereas opal is the major phase for Pa scavenging (Chase et al., 2002; Scholten et al., 2005).

The size classes <2 µm and <20 µm show $D(^{231}Pa/^{230}Th)$ values close to unity in spite of their high opal concentrations (55-70 %). These particle fractions contain the highest concentrations of both $^{231}Pa_{xs}$ (Figure 1) and $^{230}Th_{xs}$ (Table A1). Assuming the most extreme case to explain this observation, virtually all ^{231}Pa could be scavenged by opal particles, and virtually all ^{230}Th could be scavenged by clay minerals. The actual contribution of the individual particle types to total ^{231}Pa and ^{230}Th, however, cannot be fully resolved here and must be addressed in further investigations.

4. CONCLUSIONS

Within various studies the biogenic opal was suggested to be the major influencing factor for $^{231}Pa_{xs}$ and ^{10}Be scavenging in the water column. Our data show that $^{231}Pa_{xs}$ and ^{10}Be remain strongly associated to the opal-rich particles even after burial in the sediment. The fractionation from $^{230}Th_{xs}$ by opal-rich particles is more pronounced for $^{231}Pa_{xs}$ than for ^{10}Be. In congruence with previous studies we can conclude that opal fluxes in sediments are better recorded by $^{231}Pa_{xs}$ than by ^{10}Be. Our data support the view of Frank et al. (2000) who conclude from observations on the same sediment core (PS1768-8) that the ^{10}Be flux rate is not a suitable tracer for biogenic particle flux in the Southern Ocean. Owing to its sensitivity to both lithogenic particle flux and biogenic opal flux ^{10}Be should be used as tracer for total particle fluxes and its application should be restricted to situations where oceanic particle composition does not change significantly over time.

The particle specific $^{10}Be/Be$ ratios reveal that the opal-rich particles reflect a local ^{10}Be signal derived from sea surface, whereas the maximum ^{10}Be concentrations and $^{10}Be/Be$ ratios within the fine particles <20 µm point to another ^{10}Be source, possibly adsorbed to clay, equilibrated with deep water masses, and advected by bottom currents.

Our experiments have shown that biogenic opal fractionates ^{231}Pa and ^{230}Th. In regions of high latitudes where biogenic opal dominates the particle fluxes the scavenging efficiency of ^{231}Pa is increased relative to ^{230}Th. Therefore, $^{231}Pa/^{230}Th$ is not a reliable proxy for total particle flux in the Southern Ocean. However, based on our data we confirm that $^{231}Pa_{xs}$ is as reasonable tracer for opal fluxes into the Southern Ocean sediments as recently applied by Anderson et al. (2009) and Bradtmiller et al. (2009).

Many studies have applied the $^{231}Pa_{xs}/^{230}Th_{xs}$ and $^{10}Be/^{230}Th_{xs}$ ratios for paleoceanographic reconstructions on sediments deposited under rapid accumulation, making the assumption that isotope ratios are not influenced by accumulation rate and sediment

transport. Our results partly confirm this assumption, because concentrations and ratios appear to be insensitive to local variations in the focusing intensity. Based on our data, the fractionation of ^{231}Pa, ^{10}Be, and ^{230}Th by transport processes appears unlikely at our Southern Ocean study site. A definite conclusion, however, cannot be drawn as we do not have data from a corresponding winnowing site.

The simulation of winnowing (Figure 4) shows that particle sorting could change isotope ratios. An extreme sediment winnowing (removal of 70-80 % of fines) would remove high ^{231}Pa/^{230}Th and ^{10}Be/^{230}Th ratios that are associated to the hydrodynamically mobile opal-rich sediment fraction whereas the corresponding low isotope ratios are left behind associated to the hydrodynamically stationary sediment fraction.

This study shows the potential effect of particle composition and redistribution on sediment ^{231}Pa/^{230}Th which must be taken into account for the reconstructions of the Atlantic meridional overturning circulation. In case of drift deposits and sediments with high opal concentrations the use of ^{231}Pa/^{230}Th as kinematic proxy should be avoided.

The compound-specific information about $^{231}Pa_{xs}$/$^{230}Th_{xs}$ and ^{10}Be/$^{230}Th_{xs}$, which we determined here, shows the potential to trace the origin of an isotopic signature better than the previously accessible bulk isotope ratios. This allows to a certain extent to discriminate signals of remote origin and local signals from surface waters.

Acknowledgements. We thank Allan Davidson (NERC CIAF) and Ingrid Stimac (AWI) for their help in the lab, and Rainer Gersonde for providing the sediment samples. The funding for this work was provided by a Helmholtz University Young Investigators Group grant to GM. NERC granted financial support to WG for the AMS analyses at SUERC (project 9040.1007). The DAAD (project D/08/40703) funded the stay abroad for SK participating in the ^{10}Be sample preparation at the NERC CIAF. Comments by S. Krishnaswami, M. Frank and two anonymous reviewers helped improving the ma

References

Anderson R. F., Bacon M. P. and Brewer P. G. (1983a) Removal of ^{230}Th and ^{231}Pa at ocean margins. *Earth and Planetary Science Letters* **66**, 73-90. doi:10.1016/0012-821X(83)90127-9

Anderson R. F., Bacon M. P. and Brewer P. G. (1983b) Removal of ^{230}Th and ^{231}Pa from the open ocean. *Earth and Planetary Science Letters* **62**, 7-23. doi:10.1016/0012-821X(83)90067-5

Anderson R. F., Lao Y., Broecker W. S., Trumbore S. E., Hofmann H. J. and Wölfli W. (1990) Boundary Scavenging in the Pacific Ocean - A Comparison of ^{10}Be and ^{231}Pa. *Earth and Planetary Science Letters* **96**, 287-304. doi:10.1016/0012-821X(90)90008-L

Anderson R. F., Fleisher M. Q., Biscaye P. E., Kumar N., Dittrich B., Kubik P. and Suter M. (1994) Anomalous boundary scavenging in the Middle Atlantic Bight: evidence from ^{230}Th, ^{231}Pa, ^{10}Be and ^{210}Pb. *Deep Sea Research Part II: Topical Studies in Oceanography* **41**, 537-561. doi:10.1016/0967-0645(94)90034-5

Anderson R. F., Kumar N., Mortlock R. A., Froelich P. N., Kubik P., Dittrich-Hannen B. and Suter M. (1998) Late-Quaternary changes in productivity of the Southern Ocean. *Journal of Marine Systems* **17**, 497-514. doi:10.1016/S0924-7963(98)00060-8

Anderson R. F., Ali S., Bradtmiller L. I., Nielsen S. H. H., Fleisher M. Q., Anderson B. E. and Burckle L. H. (2009) Wind-Driven Upwelling in the Southern Ocean and the Deglacial Rise in Atmospheric CO_2. *Science* **323**, 1443-1448. doi:10.1126/science.1167441

Asmus T., Frank M., Koschmieder C., Frank N., Gersonde R., Kuhn G. and Mangini A. (1999) Variations of biogenic particle flux in the southern Atlantic section of the

Subantarctic Zone during the late Quaternary: Evidence from sedimentary $^{231}Pa_{ex}$ and $^{230}Th_{ex}$. *Marine Geology* **159**, 63-78. doi:10.1016/S0025-3227(98)00199-6

Bacon M. P. (1984) Glacial to Interglacial Changes in Carbonate and Clay Sedimentation in the Atlantic-Ocean Estimated from Th-230 Measurements. *Isotope Geoscience* **2**, 97-111.

Barg E., Lal D., Pavich M. J., Caffee M. W. and Southon J. R. (1997) Beryllium geochemistry in soils: evaluation of $^{10}Be/^{9}Be$ ratios in authigenic minerals as a basis for age models. *Chemical Geology* **140**, 237-258. doi:10.1016/S0009-2541(97)00051-X

Bourles D. L., Raisbeck G. M. and Yiou F. (1989) ^{10}Be and ^{9}Be in marine sediments and their potential for dating. *Geochimica et Cosmochimica Acta* **53**, 443-452. doi:10.1016/0016-7037(89)90395-5

Bradtmiller L. I., Anderson R. F., Fleisher M. Q. and Burckle L. H. (2007) Opal burial in the equatorial Atlantic Ocean over the last 30 ka: Implications for glacial-interglacial changes in the ocean silicon cycle. *Paleoceanography* **22**, PA4216. doi:10.1029/2007PA001443

Bradtmiller L. I., Anderson R. F., Fleisher M. Q. and Burckle L. H. (2009) Comparing glacial and Holocene opal fluxes in the Pacific sector of the Southern Ocean. *Paleoceanography* **24**, PA2214. doi:10.1029/2008PA001693

Brunauer S., Emmett P. H. and Teller E. (1938) Adsorption of Gases in Multimolecular Layers. *Journal of the American Chemical Society* **60**, 309-319.

Burke A., Marchal O., Bradtmiller L. I., McManus J. F. and François R. (2011) Application of an inverse method to interpret $^{231}Pa/^{230}Th$ observations from marine sediments. *Paleoceanography* **26**, PA1212. doi:10.1029/2010PA002022

Chase Z., Anderson R. F., Fleisher M. Q. and Kubik P. W. (2002) The influence of particle composition and particle flux on scavenging of Th, Pa and Be in the ocean. *Earth and Planetary Science Letters* **204**, 215-229. doi:10.1016/S0012-821X(02)00984-6

Chase Z., Anderson R. F., Fleisher M. Q. and Kubik P. W. (2003) Scavenging of ^{230}Th, ^{231}Pa and ^{10}Be in the Southern Ocean (SW Pacific sector): the importance of particle flux, particle composition and advection *Deep Sea Research Part II: Topical Studies in Oceanography* **50**, 739-768. doi:10.1016/S0967-0645(02)00593-3

Chase Z. and Anderson R. F. (2004) Comment on "On the importance of opal, carbonate, and lithogenic clays in scavenging and fractionating ^{230}Th, ^{231}Pa and ^{10}Be in the ocean" by S. Luo and T.-L. Ku. *Earth and Planetary Science Letters* **220**, 213-222. doi:10.1016/S0012-821X(04)00028-7

Christl M., Mangini A. and Kubik P. W. (2007) Highly resolved Beryllium-10 record from ODP Site 1089 - A global signal? *Earth and Planetary Science Letters* **257**, 245-258. doi:10.1016/j.epsl.2007.02.035

Christl M., Lippold J., Steinhilber F., Bernsdorff F. and Mangini A. (2010) Reconstruction of global ^{10}Be production over the past 250 ka from highly accumulating Atlantic drift sediments. *Quaternary Science Reviews* **29**, 2663-2672. doi:10.1016/j.quascirev.2010.06.017

Diekmann B., Petschick R., Gingele F. X., Fütterer D. K., Abelmann A., Brathauer U., Gersonde R. and Mackensen A. (1996) Clay mineral fluctuations in Late Quaternary sediments of the southeastern South Atlantic: Implications for past changes of deep water advection. In: G. Wefer, W. H. Berger, G. Siedler, and D. J. Webb (Eds.), *South Atlantic - Present and Past Circulation*. Springer-Verlag Berlin, Berlin. 621-644

Dutay J. C., Lacan F., Roy-Barman M. and Bopp L. (2009) Influence of particle size and type on ^{231}Pa and ^{230}Th simulation with a global coupled biogeochemical-ocean general

circulation model: A first approach. *Geochemistry Geophysics Geosystems* **10**, Q01011. doi:10.1029/2008GC002291

Finkel R., Krishnaswami S. and Clark D. L. (1977) ^{10}Be in Arctic Ocean sediments. *Earth and Planetary Science Letters* **35**, 199-204.

François R., Bacon M. P., Altabet M. A. and Labeyrie L. D. (1993) Glacial/Interglacial Changes in Sediment Rain Rate in the SW Indian Sector of Subantarctic Waters as Recorded by ^{230}Th, ^{231}Pa, U, and delta ^{15}N. *Paleoceanography* **8**, 611-629. doi:10.1029/93PA00784

François R., Frank M., Rutgers van der Loeff M. M. and Bacon M. P. (2004) ^{230}Th normalization: An essential tool for interpreting sedimentary fluxes during the late Quaternary *Paleoceanography* **19**, doi:10.1029/2003PA000939.

Frank M., Mangini A., Gersonde R., Rutgers van der Loeff M. and Kuhn G. (1996) Late Quaternary sediment dating and quantification of lateral sediment redistribution applying $^{230}Th_{ex}$: a study from the eastern Atlantic sector of the Southern Ocean. *Geologische Rundschau* **85**, 554-566. doi:10.1007/BF02369010

Frank M., Schwarz B., Baumann S., Kubik P. W., Suter M. and Mangini A. (1997) A 200 kyr record of cosmogenic radionuclide production rate and geomagnetic field intensity from ^{10}Be in globally stacked deep-sea sediments. *Earth and Planetary Science Letters* **149**, 121-129. doi:10.1016/S0012-821X(97)00070-8

Frank M. (2000) Comparison of cosmogenic radionuclide production and geomagnetic field intensity over the last 200 000 years. *Phil. Trans R. Soc. Lond. A* **358**, 1089-1107. doi:10.1098/rsta.2000.0575

Frank M., Gersonde R., Rutgers van der Loeff M., Bohrmann G., Nürnberg C. C., Kubik P., Suter M. and Mangini A. (2000) Similar glacial and interglacial export bioproductivity in the Atlantic sector of the Southern Ocean: Multiproxy evidence and implications for glacial atmospheric CO_2 *Paleoceanography* **15**, 642-658. doi:10.1029/2000PA000497

Frank M., Rutgers van der Loeff M. M., Kubik P. W. and Mangini A. (2002) Quasi-conservative behaviour of ^{10}Be in deep waters of the Weddell Sea and the Atlantic sector of the Antarctic Circumpolar Current. *Earth and Planetary Science Letters* **201**, 171-186. doi:10.1016/S0012-821X(02)00688-X

Frank M., Backman J., Jakobsson M., Moran K., O'Regan M., King J., Haley B. A., Kubik P. W. and Garbe-Schönberg D. (2008) Beryllium isotopes in central Arctic Ocean sediments over the past 12.3 million years: Stratigraphic and paleoclimatic implications. *Paleoceanography* **23**, PA1S02. doi:10.1029/2007PA001478

Freeman S., Bishop P., Bryant C., Cook G., Dougans D., Ertunc T., Fallick A., Ganeshram R., Maden C., Naysmith P., Schnabel C., Scott M., Summerfield M. and Xu S. (2007) The SUERC AMS laboratory after 3 years. *Nuclear Instruments and Methods in Physics Research Section B: Beam Interactions with Materials and Atoms* **259**, 66-70. doi:10.1016/j.nimb.2007.01.312

Geibert W. and Usbeck R. (2004) Adsorption of thorium and protactinium onto different particle types: experimental findings. *Geochimica et Cosmochimica Acta* **68**, 1489-1501. doi:10.1016/j.gca.2003.10.011

Geibert W., Rutgers van der Loeff M. M., Usbeck R., Gersonde R., Kuhn G. and Seeberg-Elverfeldt J. (2005) Quantifying the opal belt in the Atlantic and southeast Pacific sector of the Southern Ocean by means of ^{230}Th normalization. *Global Biogeochemical Cycles* **19**, GB4001. doi:10.1029/2005GB002465

Gersonde R. and Hempel G. (1990) Die Expedition ANTARKTIS-VIII/3 und VIII/4 mit FS "Polarstern" 1989. *Berichte zur Polarforschung* **74**, 173 pp. doi:10013/epic.10074.d001

Gherardi J. M., Labeyrie L., Nave S., Francois R., McManus J. F. and Cortijo E. (2009) Glacial-interglacial circulation changes inferred from ^{231}Pa/^{230}Th sedimentary record

in the North Atlantic region. *Paleoceanography* **24**, PA2204. doi:10.1029/2008PA001696

Gil I. M., Keigwin L. D. and Abrantes F. G. (2009) Deglacial diatom productivity and surface ocean properties over the Bermuda Rise, northeast Sargasso Sea. *Paleoceanography* **24**, PA4101. doi:10.1029/2008PA001729

Goel P. S. (1969) Production Rate of ^{10}Be from Oxygen Spallation. *Nature* **223**, 1263-1264. doi:10.1038/2231263a0

Guihou A., Pichat S., Nave S., Govin A., Labeyrie L., Michel E. and Waelbroeck C. (2010) Late slowdown of the Atlantic Meridional Overturning Circulation during the Last Glacial Inception: New constraints from sedimentary (^{231}Pa/^{230}Th). *Earth and Planetary Science Letters* **289**, 520-529. doi:10.1016/j.epsl.2009.11.045

Guihou A., Pichat S., Govin A., Nave S., Michel E., Duplessy J.-C., Telouk P. and Labeyrie L. (in press) Enhanced Atlantic Meridional Overturning Circulation supports the Last Glacial Inception. *Quaternary Science Reviews*. doi:10.1016/j.quascirev.2011.03.017

Guo L. D., Chen M. and Gueguen C. (2002) Control of Pa/Th ratio by particulate chemical composition in the ocean. *Geophysical Research Letters* **29**. doi:10.1029/2002GL015666

Hansen R. G. and Ring E. J. (1983) *The Preparation and Certification of a Uranium reference material*. Council for Mineral Technology, Randburg, South Africa.

Henderson G. M., Heinze C., Anderson R. F. and Winguth A. M. E. (1999) Global distribution of the ^{230}Th flux to ocean sediments constrained by GCM modelling. *Deep Sea Research Part I: Oceanographic Research Papers* **46**, 1861-1893. doi:10.1016/S0967-0637(99)00030-8

Henderson G. M. and Anderson R. F. (2003) The U-series toolbox for paleoceanography. In: B. Bourdon, G. M. Henderson, C. C. Lundstrom, and S. P. Turner (Eds.), *Uranium-Series Geochemistry*. Mineralogical Society of America, Washington. 493-531

Henderson G. M., Anderson R. F., Adkins J., Andersson P., Boyle E. A., Cutter G., de Baar H., Eisenhauer A., Frank M., Francois R., Orians K., Gamo T., German C., Jenkins W., Moffett J., Jeandel C., Jickells T., Krishnaswami S., Mackey D., Measures C. I., Moore J. K., Oschlies A., Pollard R., van der Loeff M. R. D., Schlitzer R., Sharma M., von Damm K., Zhang J. and Masque P. (2007) GEOTRACES - An international study of the global marine biogeochemical cycles of trace elements and their isotopes. *Chemie Der Erde-Geochemistry* **67**, 85-131. doi:10.1016/j.chemer.2007.02.001

Henken-Mellies W. U., Beer J., Heller F., Hsü K. J., Shen C., Bonani G., Hofmann H. J., Suter M. and Wölfli W. (1990) ^{10}Be and ^{9}Be in South Atlantic DSDP Site 519: Relation to geomagnetic reversals and to sediment composition. *Earth and Planetary Science Letters* **98**, 267-276. doi:10.1016/0012-821X(90)90029-W

ISO9277 Determination of the specific surface area of solids by gas adsorption - BET method.

Keigwin L. D. and Boyle E. A. (2008) Did North Atlantic overturning halt 17,000 years ago? *Paleoceanography* **23**, PA1101. doi:10.1029/2007PA001500

Kretschmer S., Geibert W., Rutgers van der Loeff M. M. and Mollenhauer G. (2010) Grain size effects on $^{230}Th_{xs}$ inventories in opal-rich and carbonate-rich marine sediments. *Earth and Planetary Science Letters* **294**, 131-142. doi:10.1016/j.epsl.2010.03.021

Krishnaswami S. (1976) Authigenic transition elements in Pacific pelagic clays. *Geochimica et Cosmochimica Acta* **40**(4), 425-434. doi:10.1016/0016-7037(76)90007-7

Ku T. L., Kusakabe M., Measures C. I., Southon J. R., Cusimano G., Vogel J. S., Nelson D. E. and Nakaya S. (1990) Beryllium isotope distribution in the western North Atlantic: a comparison to the Pacific. *Deep Sea Research Part A. Oceanographic Research Papers* **37**, 795-808. doi:10.1016/0198-0149(90)90007-I

Kumar N., Gwiazda R., Anderson R. F. and Froelich P. N. (1993) $^{231}Pa/^{230}Th$ ratios in sediments as a proxy for past changes in Southern Ocean productivity. *Nature* **362**, 45-48. doi:10.1038/362045a0

Kumar N., Anderson R. F., Mortlock R. A., Froelich P. N., Kubik P., Dittrich-Hannen B. and Suter M. (1995) Increased biological productivity and export production in the glacial Southern Ocean. *Nature* **378**, 675-680. doi:10.1038/378675a0

Kusakabe M., Ku T. L., Vogel J., Southon J. R., Nelson D. E. and Richards G. (1982) ^{10}Be profiles in seawater. *Nature* **299**, 712-714. doi:10.1038/299712a0

Kusakabe M., Ku T. L., Southon J. R., Vogel J. S., Nelson D. E., Measures C. I. and Nozaki Y. (1987) Distribution of ^{10}Be and ^{9}Be in the Pacific Ocean. *Earth and Planetary Science Letters* **82**, 231-240. doi:10.1016/0012-821X(87)90198-1

Lal D. and Peters B. (1967) Cosmic ray produced radioactivity on the Earth. In *Handbuch der Physik*, Vol. **46** (ed. S. Fluegge and K. Sitte), pp. 551-612. Springer-Verlag.

Lal D. (2002) Cosmogenic Radionuclides. In *Encyclopedia of Atmospheric Sciences* (eds. J. R. Holton, J. A. Curry, and J. A. Pyle), pp. 1891-1900. Academic Press.

Lal D., Charles C., Vacher L., Goswami J. N., Jull A. J. T., McHargue L. and Finkel R. C. (2006) Paleo-ocean chemistry records in marine opal: Implications for fluxes of trace elements, cosmogenic nuclides (^{10}Be and ^{26}Al), and biological productivity. *Geochimica et Cosmochimica Acta* **70**, 3275-3289. doi:10.1016/j.gca.2006.04.004

Langmuir D. and Herman J. S. (1980) The mobility of thorium in natural waters at low temperatures. *Geochimica et Cosmochimica Acta* **44**, 1753-1766. doi:10.1016/0016-7037(80)90226-4

Lao Y., Anderson R. F., Broecker W. S., Trumbore S. E., Hofmann H. J. and Wölfli W. (1992) Transport and burial rates of ^{10}Be and ^{231}Pa in the Pacific Ocean during the Holocene period. *Earth and Planetary Science Letters* **113**, 173-189. doi:10.1016/0012-821X(92)90218-K

Lao Y., Anderson R. F., Broecker W. S., Hofmann H. J. and Wölfli W. (1993) Particulate fluxes of ^{230}Th, ^{231}Pa, and ^{10}Be in the northeastern Pacific Ocean. *Geochimica et Cosmochimica Acta* **57**, 205-217. doi:10.1016/0016-7037(93)90479-G

Lippold J., Grützner J., Winter D., Lahaye Y., Mangini A. and Christl M. (2009) Does sedimentary ^{231}Pa/^{230}Th from the Bermuda Rise monitor past Atlantic Meridional Overturning Circulation? *Geophysical Research Letters* **36**, L12601. doi:10.1029/2009GL038068

Luo S. and Ku T.-L. (1999) Oceanic ^{231}Pa/^{230}Th ratio influenced by particle composition and remineralization. *Earth and Planetary Science Letters* **167**, 183-195. doi:10.1016/S0012-821X(99)00035-7

Luo S. and Ku T.-L. (2003) Constraints on deep-water formation from the oceanic distributions of ^{10}Be. *J. Geophys. Res.* **108**, 3137. doi:10.1029/2002JC001670

Luo S. and Ku T.-L. (2004a) Reply to Comment on "On the importance of opal, carbonate, and lithogenic clays in scavenging and fractionating ^{230}Th, ^{231}Pa and ^{10}Be in the ocean". *Earth and Planetary Science Letters* **220**, 223-229. doi:10.1016/S0012-821X(04)00029-9

Luo S. and Ku T.-L. (2004b) On the importance of opal, carbonate, and lithogenic clays in scavenging and fractionating ^{230}Th, ^{231}Pa and ^{10}Be in the ocean. *Earth and Planetary Science Letters* **220**, 201-211. doi:10.1016/S0012-821X(04)00027-5

Luo Y., Francois R. and Allen S. E. (2010) Sediment ^{231}Pa/^{230}Th as a recorder of the rate of the Atlantic meridional overturning circulation: insights from a 2-D model. *Ocean Science* **6**, 381-400. doi:10.5194/os-6-381-2010

Martínez-Garcia A., Rosell-Melé A., Geibert W., Gersonde R., Masqué P., Gaspari V. and Barbante C. (2009) Links between iron supply, marine productivity, sea surface temperature, and CO_2 over the last 1.1 Ma. *Paleoceanography* **24**, PA1207. doi:10.1029/2008PA001657

McCave I. N., Manighetti B. and Robinson S. G. (1995) Sortable Silt and Fine Sediment Size/Composition Slicing: Parameters for Palaeocurrent Speed and Palaeoceanography. *Paleoceanography* **10**. doi:10.1029/94PA03039

McManus J. F., Francois R., Gherardi J. M., Keigwin L. D. and Brown-Leger S. (2004) Collapse and rapid resumption of Atlantic meridional circulation linked to deglacial climate changes. *Nature* **428**, 834-837. doi:10.1038/nature02494

Middleton R., Brown L., Dezfouly-Arjomandy B. and Klein J. (1993) On ^{10}Be standards and the half-life of ^{10}Be. *Nuclear Instruments and Methods in Physics Research Section B: Beam Interactions with Materials and Atoms* **82**, 399-403. doi:10.1016/0168-583X(93)95987-G

Monaghan M. C., Krishnaswami S. and Turekian K. K. (1986) The global-average production rate of ^{10}Be. *Earth and Planetary Science Letters* **76**, 279-287. doi:10.1016/0012-821X(86)90079-8

Moore R. M. and Hunter K. A. (1985) Thorium adsorption in the ocean: reversibility and distribution amongst particle sizes. *Geochimica et Cosmochimica Acta* **49**, 2253-2257. doi:10.1016/0016-7037(85)90225-X

Moore R. M. and Millward G. E. (1988) The kinetics of reversible Th reactions with marine particles. *Geochimica et Cosmochimica Acta* **52**, 113-118. doi:10.1016/0016-7037(88)90060-9

Morris J. D., Gosse J., Brachfeld S. and Tera F. (2002) Cosmogenic Be-10 and the Solid Earth: Studies in Geomagnetism, Subduction Zone Processes, and Active Tectonics. In: E. S. Grew (Ed.), *Beryllium: Mineralogy, Petrology, and Geochemistry*. Mineralogical Society of America, Washington. 207-270

Müller P. J. and Schneider R. (1993) An automated leaching method for the determination of opal in sediments and particulate matter. *Deep Sea Research Part I: Oceanographic Research Papers* **40**, 425-444. doi:10.1016/0967-0637(93)90140-X

Negre C., Zahn R., Thomas A. L., Masqué P., Henderson G. M., Martinez-Mendez G., Hall I. R. and Mas J. L. (2010) Reversed flow of Atlantic deep water during the Last Glacial Maximum. *Nature* **468**, 84-88. doi:10.1038/nature09508

Niven S. E. H. and Moore R. M. (1993) Thorium sorption in seawater suspensions of aluminium oxide particles. *Geochimica et Cosmochimica Acta* **57**, 2169-2179. doi:10.1016/0016-7037(93)90558-E

Pichat S., Sims K. W. W., François R., McManus J. F., Brown Leger S. and Albarède F. (2004) Lower export production during glacial periods in the equatorial Pacific derived from $(^{231}Pa/^{230}Th)_{xs,0}$ measurements in deep-sea sediments. *Paleoceanography* **19**, PA4023. doi:10.1029/2003PA000994

Robinson L. F., Belshaw N. S. and Henderson G. M. (2004) U and Th concentrations and isotope ratios in modern carbonates and waters from the Bahamas. *Geochimica et Cosmochimica Acta* **68**, 1777-1789. doi:10.1016/j.gca.2003.10.005

Robinson L. F., Noble T. L. and McManus J. F. (2008) Measurement of adsorbed and total $^{232}Th/^{230}Th$ ratios from marine sediments. *Chemical Geology* **252**, 169-179. doi:10.1016/j.chemgeo.2008.02.015

Roy-Barman M., Jeandel C., Souhaut M., Rutgers van der Loeff M., Voege I., Leblond N. and Freydier R. (2005) The influence of particle composition on thorium scavenging in the NE Atlantic ocean (POMME experiment). *Earth and Planetary Science Letters* **240**, 681-693. doi:10.1016/j.epsl.2005.09.059

Roy-Barman M., Lemaître C., Ayrault S., Jeandel C., Souhaut M. and Miquel J. C. (2009) The influence of particle composition on Thorium scavenging in the Mediterranean Sea. *Earth and Planetary Science Letters* **286**, 526-534. doi:10.1016/j.epsl.2009.07.018

Rutgers van der Loeff M. M. and Berger G. W. (1993) Scavenging of ^{230}Th and ^{231}Pa near the antarctic polar front in the South Atlantic. *Deep Sea Research Part I: Oceanographic Research Papers* **40**, 339-357. doi:10.1016/0967-0637(93)90007-P

Scholten J. C., Fietzke J., Vogler S., Rutgers van der Loeff M. M., Mangini A., Koeve W., Waniek J., Stoffers P., Antia A. and Kuss J. (2001) Trapping efficiencies of sediment traps from the deep Eastern North Atlantic:: The ^{230}Th calibration. *Deep Sea Research Part II: Topical Studies in Oceanography* **48**, 2383-2408. doi:10.1016/S0967-0645(00)00176-4

Scholten J. C., Fietzke J., Mangini A., Stoffers P., Rixen T., Gaye-Haake B., Blanz T., Ramaswamy V., Sirocko F., Schulz H. and Ittekkot V. (2005) Radionuclide fluxes in the Arabian Sea: the role of particle composition. *Earth and Planetary Science Letters* **230**, 319-337. doi:10.1016/j.epsl.2004.11.003

Scholten J. C., Fietzke J., Mangini A., Garbe-Schönberg C. D., Eisenhauer A., Schneider R. and Stoffers P. (2008) Advection and scavenging: Effects on ^{230}Th and ^{231}Pa distribution off Southwest Africa. *Earth and Planetary Science Letters* **271**, 159-169. doi:10.1016/j.epsl.2008.03.060

Siddall M., Henderson G. M., Edwards N. R., Frank M., Müller S. A., Stocker T. F. and Joos F. (2005) ^{231}Pa / ^{230}Th fractionation by ocean transport, biogenic particle flux and particle type. *Earth and Planetary Science Letters* **237**, 135-155. doi:10.1016/j.epsl.2005.05.031

Suman D. O. and Bacon M. P. (1989) Variations in Holocene sedimentation in the North American Basin determined from ^{230}Th measurements. *Deep Sea Research Part A. Oceanographic Research Papers* **36**, 869-878. doi:10.1016/0198-0149(89)90033-2

Taguchi K., Harada K. and Tsunogai S. (1989) Particulate removal of ^{230}Th and ^{231}Pa in the biologically productive northern North Pacific. *Earth and Planetary Science Letters* **93**, 223-232. doi:10.1016/0012-821X(89)90070-8

Walter H. J., Rutgers van der Loeff M. M. and Hoeltzen H. (1997) Enhanced scavenging of ^{231}Pa relative to ^{230}Th in the South Atlantic south of the Polar Front: Implications for the use of the ^{231}Pa/^{230}Th ratio as a paleoproductivity proxy. *Earth and Planetary Science Letters* **149**, 85-100. doi:10.1016/S0012-821X(97)00068-X

Wang L., Ku T. L., Luo S., Southon J. R. and Kusakabe M. (1996) ^{26}Al-^{10}Be systematics in deep-sea sediments. *Geochimica et Cosmochimica Acta* **60**, 109-119. doi:10.1016/0016-7037(95)00379-7

Xu S., Dougans A. B., Freeman S. P. H. T., Schnabel C. and Wilcken K. M. (2010) Improved ^{10}Be and ^{26}Al-AMS with a 5 MV spectrometer. *Nuclear Instruments and Methods in Physics Research Section B: Beam Interactions with Materials and Atoms* **268**, 736-738. doi:10.1016/j.nimb.2009.10.018

Yang H.-S., Nozaki Y., Sakai H. and Masuda A. (1986) The distribution of ^{230}Th and ^{231}Pa in the deep-sea surface sediments of the Pacific Ocean. *Geochimica et Cosmochimica Acta* **50**, 81-89. doi:10.1016/0016-7037(86)90050-5

Yu E.-F., Francois R. and Bacon M. P. (1996) Similar rates of modern and last-glacial ocean thermohaline circulation inferred from radiochemical data. *Nature* **379**, 689-694. doi:10.1038/379689a0

Tables

Table 1: Sieving recoveries and leaching loss of ^{230}Th, ^{231}Pa and ^{10}Be after the size fractionation of the sediment samples. The leaching loss is the amount of ^{230}Th, ^{231}Pa and ^{10}Be that was lost by desorption and/or dissolution during sieving/settling and remained in the supernatant water, expressed as the percentage of the total initial amount.

samples	Sediment sieved [g]	^{230}Th in sediment [dpm/g]	Recovery of ^{230}Th after sieving [%]	seawater used as sieving fluid [kg]	^{230}Th in supernatant [dpm/kg]	^{230}Th leached from sediment [dpm]	^{230}Th lost to supernatant in % of total ^{230}Th [%]
PS1768-8	7.7	6.45	87	22.49	0.05332	1.191	2.4
PS1769-1	7.9	6.09	90	19.10	0.05568	1.056	2.2
“unused” seawater				21.69	0.00037		

samples	Sediment sieved [g]	^{231}Pa in sediment [dpm/g]	Recovery of ^{231}Pa after sieving [%]	seawater used as sieving fluid [kg]	^{231}Pa in supernatant [dpm/kg]	^{231}Pa leached from sediment [dpm]	^{231}Pa lost to supernatant in % of total ^{231}Pa [%]
PS1768-8	7.7	0.83	110	22.49	0.00181	0.032	0.5
PS1769-1	7.9	0.80	109	19.10	0.00169	0.025	0.4
“unused” seawater				21.69	0.00036		

samples	AMS ID	Sediment sieved [g]	^{10}Be in sediment [at/g]	Recovery of ^{10}Be after sieving [%]	seawater used as sieving fluid [kg]	^{10}Be in supernatant [at/kg]	^{10}Be leached from sediment [at]	^{10}Be lost to supernatant in % of total ^{10}Be [%]
PS1768-8	b2692	14.4	2.54E+09	103	11.31	1.88E+07	2.09E+08	0.6
PS1769-1	b2832	18.6	2.24E+09	104	15.40	1.93E+07	2.92E+08	0.7
“unused” seawater 1	b2693				11.53	3.12E+05		
“unused” seawater 2	b2694				15.51	2.50E+05		

Table 2: Percentage contribution by particle size classes. Each size class contributes a certain fraction to the total flux of opal and particulate $^{230}Th_{xs}$, $^{231}Pa_{xs}$, ^{10}Be and Be. Expressed in percentage, the comparison between parameters is possible and the potential influence of particle size sorting on isotope ratios can be assessed.

			percentage contribution [%] to total inventory				
particle size class [µm]	settling velocity	wt-% size-fraction	opal	$^{230}Th_{xs}$	$^{231}Pa_{xs}$	^{10}Be	Be
sediment core PS1768-8							
<20		76.4	77.1	90.5	88.6	90	83.3
20-63	slow	14.7	20.3	5.9	9.3	7.4	8.8
>63	slow	2.8	1.9	1.1	1.6	1.2	1.9
20-63	fast	2.7	0.5	1.4	0.3	0.7	2.8
>63	fast	3.5	0.1	1.1	0.2	0.7	3.2
sediment core PS1769-1							
<20		72.5	74.7	90.6	87.7	90.4	81.6
20-63	slow	14.9	21.8	4.2	10	5.2	6.3
>63	slow	3	2.1	1	1.4	1.4	1.8
20-63	fast	2.6	0.8	1.8	0.4	0.9	3.8
>63	fast	7	0.6	2.5	0.5	2	6.5

fast = particles of high specific density which were isolated by their rapid settling velocity in seawater (mainly ice rafted debris)

slow = particles of low specific density which were isolated by their slow settling velocity in seawater (mainly diatoms)

Appendix

Table A1: Particle size specific activities of ^{231}Pa and ^{230}Th in two sediment samples. The size classes >20 µm are split in two particle types by their settling velocity (fast and slow) in seawater. Data on $xs^{230}Th_0$ are from Kretschmer et al. (2010). The distribution ratio *D*(Pa/Th) expresses the particle specific distribution of $xs^{231}Pa_0$ relative to the particle specific distribution of $xs^{230}Th_0$ (for explanation see text). Excess $^{231}Pa_0$ and $^{230}Th_0$ activities are decay corrected to the time of deposition at 16 ka. The uncertainty is given as 1σ. AR = activity ratio.

size class [µm]	settle velocity	^{230}Th	$xs^{230}Th_0$	^{231}Pa	$xs^{231}Pa_0$	$xsPa_0/Th_0$	D(Pa/Th)
		[dpm g^{-1}]				[AR]	
sediment core PS1768-8							
bulk		6.45 ±0.12	6.68 ±1.13	0.83 ±0.03	1.10 ±0.19	0.16 ±0.04	
<2		11.91 ±0.20	12.81 ±2.16	1.20 ±0.01	1.59 ±0.27	0.12 ±0.03	0.75 ±0.25
2-20		1.30 ±0.03	1.23 ±0.21	0.49 ±0.01	0.67 ±0.11	0.54 ±0.13	3.31 ±1.11
<20		6.58 ±0.11	6.94 ±1.17	1.05 ±0.02	1.40 ±0.24	0.20 ±0.05	1.23 ±0.41
20-63	fast	2.94 ±0.06	3.12 ±0.53	0.12 ±0.01	0.14 ±0.03	0.05 ±0.01	0.27 ±0.10
63-125	fast	2.50 ±0.05	2.68 ±0.45	0.04 ±0.00	0.03 ±0.01	0.01 ±0.00	0.07 ±0.03
>125	fast	1.39 ±0.03	1.45 ±0.25	0.06 ±0.00	0.08 ±0.01	0.05 ±0.01	0.34 ±0.11
>63	fast	1.75 ±0.04	1.84 ±0.31	0.05 ±0.00	0.06 ±0.01	0.03 ±0.01	0.20 ±0.07
20-63	slow	2.20 ±0.04	2.34 ±0.39	0.56 ±0.01	0.77 ±0.13	0.33 ±0.08	2.00 ±0.67
63-125	slow	2.01 ±0.04	2.13 ±0.36	0.53 ±0.01	0.72 ±0.12	0.34 ±0.08	2.05 ±0.70
>125	slow	3.83 ±0.08	4.19 ±0.71	0.35 ±0.01	0.46 ±0.08	0.11 ±0.03	0.67 ±0.23
>63	slow	2.12 ±0.04	2.26 ±0.38	0.52 ±0.01	0.71 ±0.12	0.31 ±0.08	1.91 ±0.65
sediment core PS1769-1							
bulk		6.09 ±0.10	6.67 ±1.13	0.80 ±0.02	1.10 ±0.19	0.16 ±0.04	
<2		11.52 ±0.19	12.73 ±2.15	1.38 ±0.03	1.89 ±0.32	0.15 ±0.04	0.90 ±0.31
2-20		2.03 ±0.04	2.14 ±0.36	0.50 ±0.01	0.68 ±0.11	0.32 ±0.08	1.93 ±0.65
<20		7.02 ±0.13	7.69 ±1.30	1.06 ±0.05	1.45 ±0.25	0.19 ±0.05	1.14 ±0.39
20-63	fast	3.91 ±0.07	4.16 ±0.70	0.15 ±0.01	0.19 ±0.03	0.05 ±0.01	0.28 ±0.10
63-125	fast	2.31 ±0.06	2.46 ±0.42	0.05 ±0.00	0.06 ±0.01	0.02 ±0.01	0.15 ±0.05
>125	fast	1.90 ±0.04	2.03 ±0.34	0.07 ±0.01	0.09 ±0.02	0.04 ±0.01	0.27 ±0.10
>63	fast	2.01 ±0.04	2.15 ±0.36	0.06 ±0.01	0.08 ±0.02	0.04 ±0.01	0.23 ±0.08
20-63	slow	1.59 ±0.03	1.74 ±0.29	0.58 ±0.02	0.81 ±0.14	0.46 ±0.11	2.82 ±0.96
63-125	slow	1.81 ±0.03	2.00 ±0.34	0.41 ±0.01	0.57 ±0.10	0.28 ±0.07	1.73 ±0.59
>125	slow	3.41 ±0.07	3.79 ±0.64	0.55 ±0.04	0.74 ±0.13	0.20 ±0.05	1.18 ±0.41
>63	slow	2.06 ±0.04	2.28 ±0.38	0.43 ±0.02	0.60 ±0.10	0.26 ±0.06	1.60 ±0.54

fast = particles of high specific density which were isolated by their rapid settling velocity in seawater (mainly ice rafted debris)
slow = particles of low specific density which were isolated by their slow settling velocity in seawater (mainly diatoms)

Table A2: Particle size specific concentrations and ratios of ^{10}Be, Be and excess ^{230}Th in two sediment samples. The size classes >20 µm are split in two particle types by their settling velocity (fast and slow) in seawater. Data on $xs^{230}Th_0$ are from Kretschmer et al. (2010). The distribution ratio *D*(Be/Th) expresses the particle specific distribution of ^{10}Be relative to the particle specific distribution of $xs^{230}Th_0$ (for explanation see text). ^{10}Be concentrations and $xs^{230}Th_0$ activities are decay corrected to the time of deposition at 16 ka. The uncertainty is given as 1σ.

AMS ID	size class [µm]	settle veloc.	$xs^{230}Th_0$ [dpm g^{-1}]	^{10}Be [10^9 at g^{-1}]	Be [µg g^{-1}]	^{10}Be/Be [10^{-8} at at^{-1}]	^{10}Be/$xs^{230}Th_0$ [10^9at dpm^{-1}]	D(Be/Th)
sediment core PS1768-8								
b2690	bulk		6.45 ±0.12	2.56 ±0.08	0.83 ±0.02	4.61 ±0.17	0.38 ±0.07	
b2688	<20		6.58 ±0.11	3.11 ±0.10	0.85 ±0.01	5.46 ±0.19	0.45 ±0.08	1.17 ±0.28
b2655	20-63	fast	2.94 ±0.06	0.69 ±0.02	0.81 ±0.00	1.26 ±0.04	0.22 ±0.04	0.58 ±0.14
b2659	>63	fast	1.75 ±0.04	0.50 ±0.02	0.72 ±0.01	1.04 ±0.03	0.27 ±0.05	0.71 ±0.17
b2689	20-63	slow	2.20 ±0.04	1.33 ±0.04	0.47 ±0.01	4.26 ±0.14	0.57 ±0.10	1.48 ±0.36
b2658	>63	slow	2.12 ±0.04	1.15 ±0.04	0.54 ±0.01	3.20 ±0.12	0.51 ±0.09	1.33 ±0.32
sediment core PS1769-1								
b2660	bulk		6.09 ±0.10	2.26 ±0.07	0.81 ±0.01	4.16 ±0.14	0.34 ±0.06	
b2661	<20		7.02 ±0.13	3.03 ±0.09	0.82 ±0.02	5.54 ±0.20	0.39 ±0.07	1.16 ±0.28
b2663	20-63	fast	3.91 ±0.07	0.86 ±0.03	1.05 ±0.02	1.23 ±0.04	0.21 ±0.04	0.61 ±0.15
b2664	>63	fast	2.01 ±0.04	0.70 ±0.02	0.68 ±0.01	1.55 ±0.05	0.33 ±0.06	0.96 ±0.23
b2662	20-63	slow	1.59 ±0.03	0.84 ±0.03	0.31 ±0.01	4.10 ±0.17	0.49 ±0.08	1.42 ±0.35
b2665	>63	slow	2.06 ±0.04	1.14 ±0.03	0.43 ±0.01	3.91 ±0.15	0.50 ±0.08	1.48 ±0.36

fast = particles of high specific density which were isolated by their rapid settling velocity in seawater (mainly ice rafted debris)

slow = particles of low specific density which were isolated by their slow settling velocity in seawater (mainly diatoms)

Table A3: Particle size specific ^{232}Th, Aluminum (Al), biogenic opal, and specific surface area (SSA) in two sediment samples. The size classes >20 µm are split in two particle types by their settling velocity (fast and slow) in seawater. Data are from Kretschmer et al. (2010). The uncertainty is given as 1σ.

size class [µm]	settle velocity	^{232}Th [dpm g^{-1}]	Al [%]	opal [%]	SSA [m^2 g^{-1}]
sediment core PS1768-8					
bulk		0.522 ±0.009	2.03 ±0.03	54.8	
<2		0.842 ±0.014	2.37 ±0.03	67.7	
2-20		0.256 ±0.004	1.38 ±0.02	75.6	
<20		0.538 ±0.009	2.05 ±0.03	54.7	
20-63	fast	0.306 ±0.005	5.81 ±0.11	14.8	
63-125	fast	0.244 ±0.004	7.30 ±0.18		
>125	fast	0.181 ±0.004	6.17 ±0.08	3.4	
>63	fast	0.201 ±0.004	6.53 ±0.12		
20-63	slow	0.138 ±0.002	0.57 ±0.02	74.9	
63-125	slow	0.106 ±0.002	0.42 ±0.01	76.0	
>125	slow	0.222 ±0.005	0.95 ±0.01		
>63	slow	0.113 ±0.002	0.45 ±0.01		
sediment core PS1769-1					
bulk		0.461 ±0.008	1.97 ±0.03	59.8	19.2
<2		0.756 ±0.012	2.31 ±0.03	61.0	56.5
2-20		0.239 ±0.004	1.17 ±0.01	79.6	13.0
<20		0.528 ±0.007	1.75 ±0.02	57.7	33.3
20-63	fast	0.507 ±0.008	5.65 ±0.11	17.5	2.7
63-125	fast	0.295 ±0.006	6.96 ±0.08	5.0	1.6
>125	fast	0.231 ±0.004	6.86 ±0.03	4.2	3.3
>63	fast	0.248 ±0.004	6.89 ±0.05	4.4	2.2
20-63	slow	0.091 ±0.002	0.35 ±0.00	81.9	11.2
63-125	slow	0.096 ±0.002	0.48 ±0.00	79.1	9.5
>125	slow	0.210 ±0.004	0.78 ±0.00		
>63	slow	0.113 ±0.002	0.53 ±0.00		

fast = particles of high specific density which were isolated by their rapid settling velocity in seawater (mainly ice rafted debris)

slow = particles of low specific density which were isolated by their slow settling velocity in seawater (mainly diatoms)

Figure captions

Figure 1: Concentrations of $^{231}Pa_{xs}$ and ^{10}Be and isotope ratios of excess $^{231}Pa/^{230}Th$ and $^{10}Be/^{230}Th$ in two sediment samples distributed by particle classes [µm]. The bulk sediment was split into size-classes by sieving. Subsequently, particles of different specific densities in size-classes >20 µm were split by their settling velocity in seawater into a rapidly settling fraction (higher density, mainly ice-rafted debris of lithogenic source) and a slowly settling fraction (lower density, mainly biogenic opal of diatoms). The error bars display the analytical uncertainty of 1σ. Grey horizontal lines indicate the production ratio of $^{231}Pa_{xs}/^{230}Th_{xs}$ (0.093) and a range of the production ratio of $^{10}Be/^{230}Th_{xs}$ (0.136-0.170 × 10^9 at dpm^{-1}). This range is based on ^{230}Th production at 3300 m water depth and a global average production of ^{10}Be at about 16 ka BP between 1.2 and 1.5 × 10^6 at cm^{-2} yr^{-1} derived from Christl et al. (2007) and Frank et al. (1997).

Figure 2: **(a)** $^{231}Pa_{xs}$ and $^{230}Th_{xs}$ specific activities [dpm g^{-1}] and ^{10}Be concentrations [10^9 at g^{-1}] in particle classes (error bar = 1σ) are plotted against the specific surface area (ssa) [m^2 g^{-1}] of the particles. **(b)** $^{231}Pa_{xs}/^{230}Th_{xs}$ [activity ratio] and $^{10}Be/^{230}Th_{xs}$ [10^9 at dpm^{-1}] in particle classes are plotted against biogenic opal [%], aluminum concentration [%] and ^{232}Th specific activity [dpm g^{-1}] (error bar = 1σ). Data and methods on specific surface area, biogenic opal content and Al concentrations are reported by Kretschmer et al. (2010).

Figure 3: The distribution ratio *D*(N/Th) (see text for definition) is calculated for each particle fraction. Values of *D* are plotted on a logarithmic scale, where $0<D<1$ indicates a fractionation that favors ^{230}Th over the radionuclide *N* (^{231}Pa or ^{10}Be), and $D>1$ indicates a fractionation that favors the radionuclide *N* (^{231}Pa or ^{10}Be) over ^{230}Th. The samples are

ordered on the x-axis with increasing biogenic opal content from left to right. Numbers above the bars indicate the particle sizes [µm].

Figure 4: Simulating the effect of winnowing on the isotope ratios **(a)** $^{231}Pa_{xs}/^{230}Th_{xs}$ and **(b)** $^{10}Be/^{230}Th_{xs}$ for the sediment sample PS1768-8. Starting with the bulk composition, the fine fraction is progressively removed and the resulting composition is calculated by using grain size and isotopic concentration data (Table 2). The resulting isotope ratio depends on the type of particles being removed: removal of only fine particles <20 µm (dashed line) leads to an increase of isotope ratios, while the combined removal of <20 µm-particles and opal-rich particles (solid line) leads to a decrease of isotope ratios.

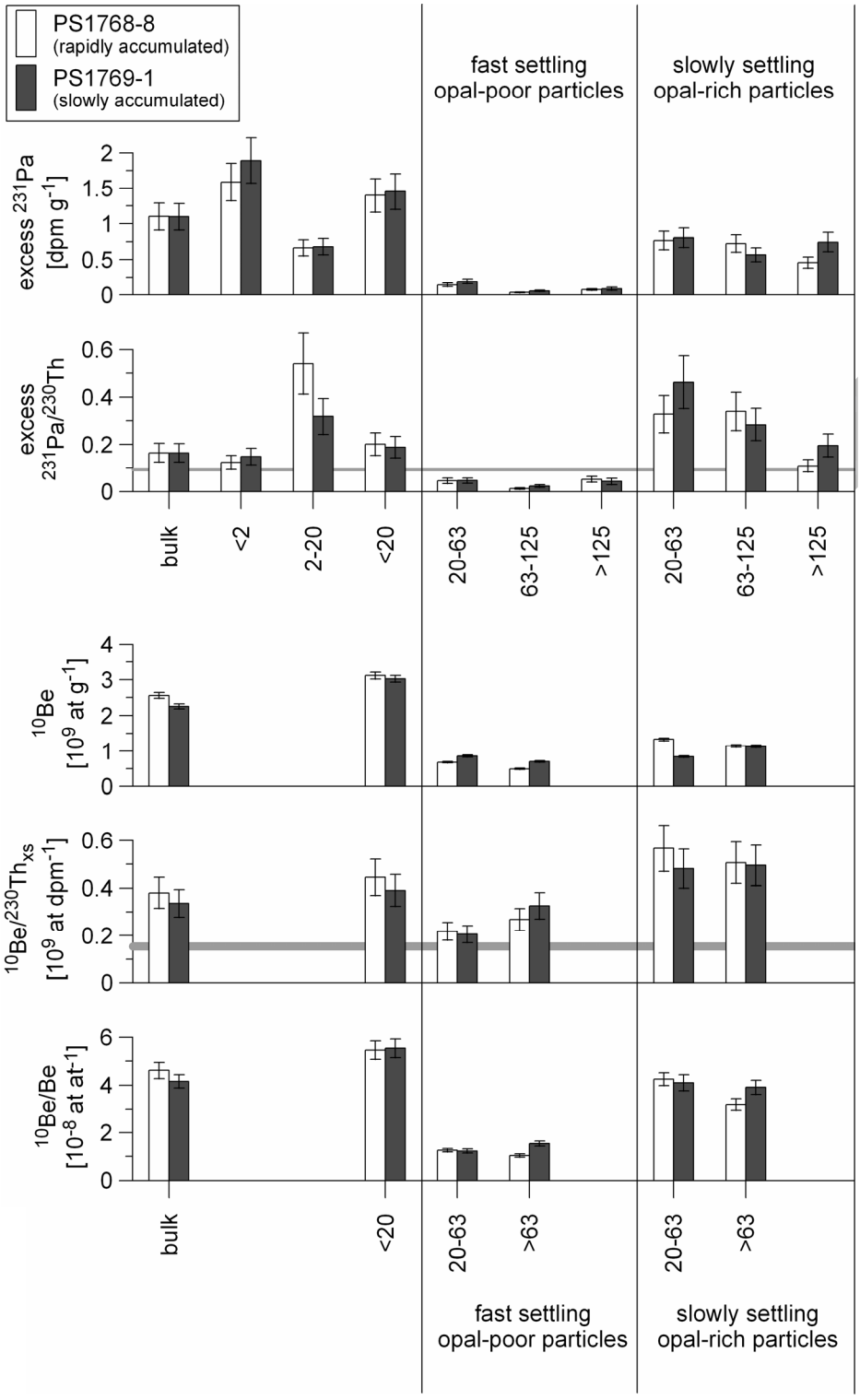
PS1768-8
(rapidly accumulated)
PS1769-1
(slowly accumulated)
fast settling
opal-poor particles
slowly settling
opal-rich particles
excess 231Pa
[dpm g-1]
excess
231Pa/230Th
10Be
[109 at g-1]
10Be/230Thxs
[109 at dpm-1]
10Be/Be
[10-8 at at-1]
bulk
<2
2-20
<20
20-63
63-125
>125
>63

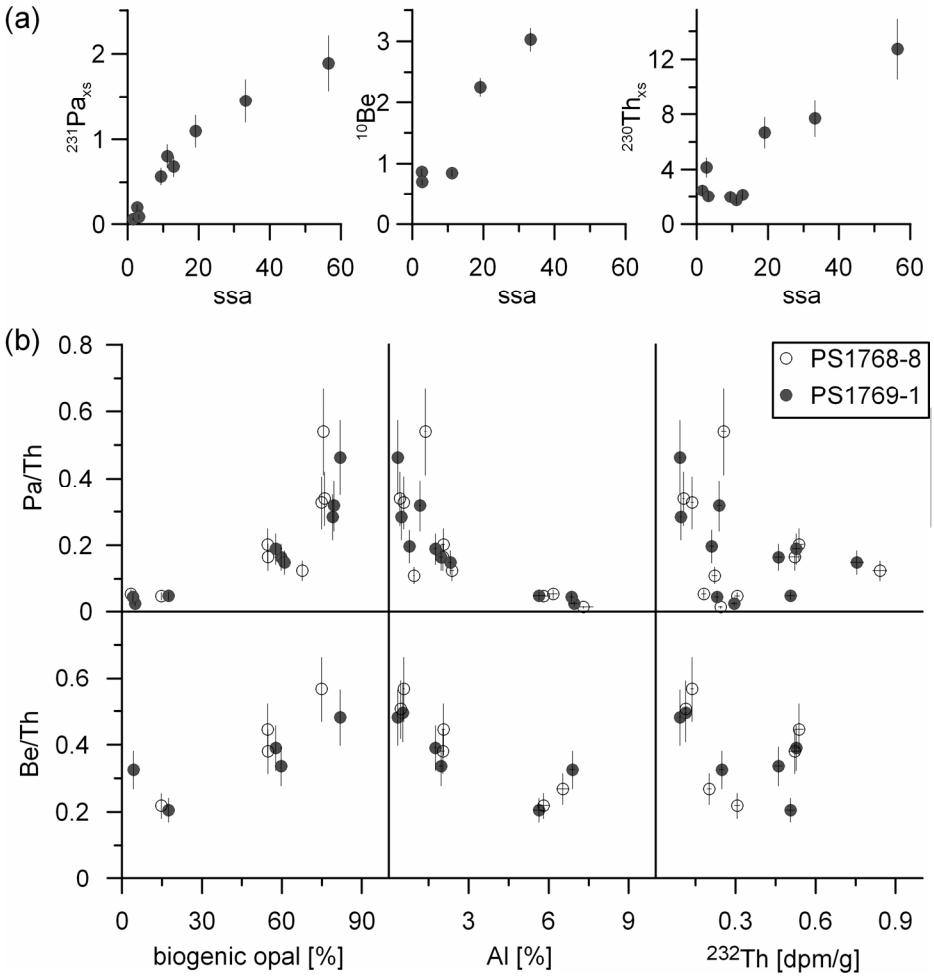
(a)
$^{231}Pa_{xs}$
^{10}Be
$^{230}Th_{xs}$
ssa
ssa
ssa
(b)
PS1768-8
PS1769-1
Pa/Th
Be/Th
biogenic opal [%]
Al [%]
^{232}Th [dpm/g]

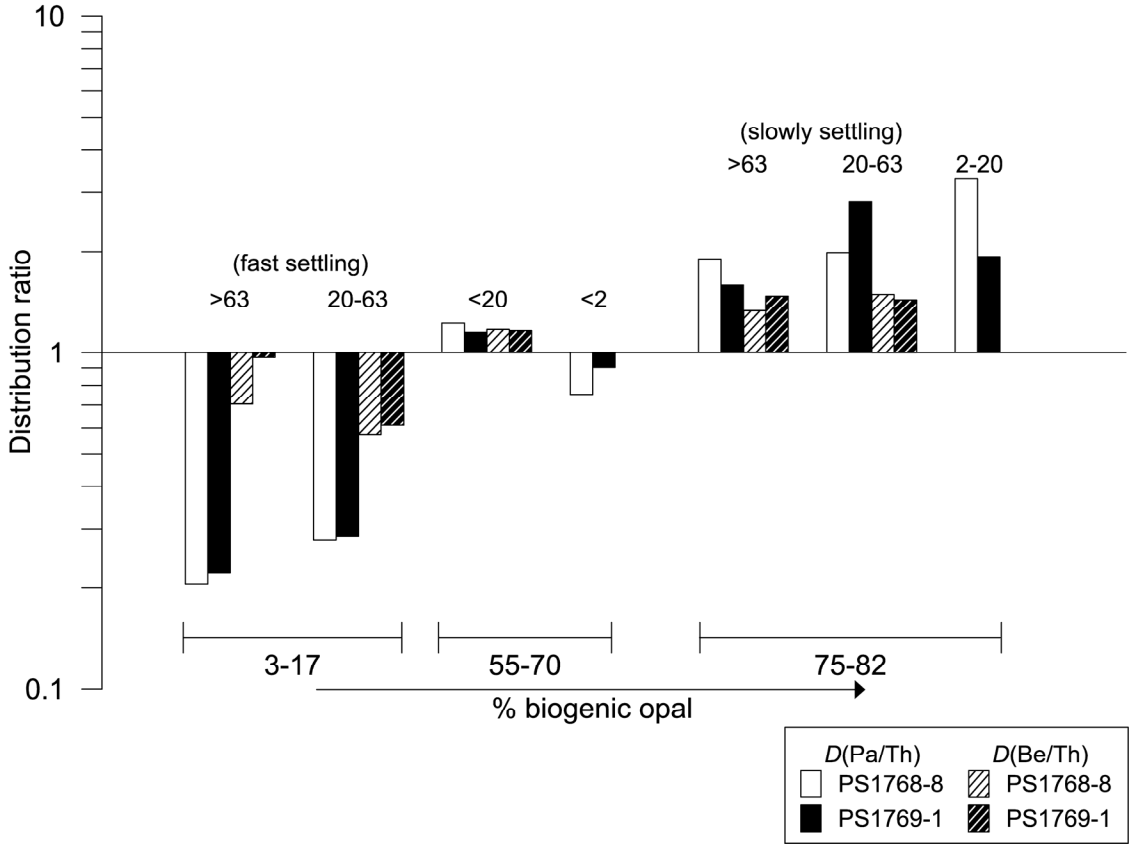
10
1
0.1
Distribution ratio
(fast settling)
>63
20-63
<20
<2
(slowly settling)
>63
20-63
2-20
3-17
55-70
75-82
% biogenic opal
D(Pa/Th)
PS1768-8
PS1769-1
D(Be/Th)
PS1768-8
PS1769-1

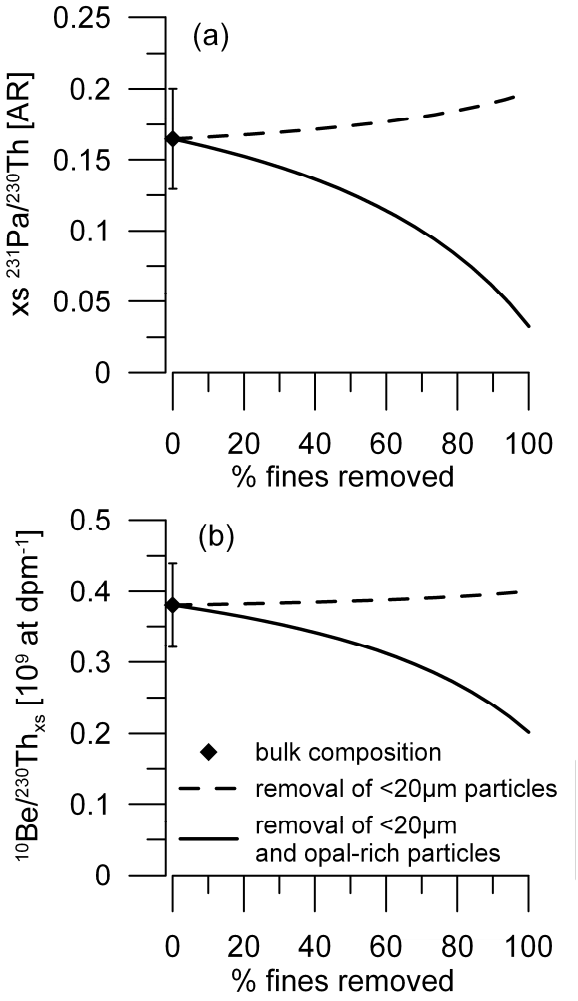
(a)
xs ^{231}Pa/^{230}Th [AR]
0.25
0.2
0.15
0.1
0.05
0
0
20
40
60
80
100
% fines removed
(b)
^{10}Be/^{230}Th$_{xs}$ [10^9 at dpm^{-1}]
0.5
0.4
0.3
0.2
0.1
0
bulk composition
removal of <20μm particles
removal of <20μm
and opal-rich particles
0
20
40
60
80
100
% fines removed